Subcellular Compartmentation of Alternatively Spliced Transcripts Defines *SERINE/ARGININE-RICH PROTEIN30* Expression[1[OPEN]]

Lisa Hartmann,[2] Theresa Wießner,[2] and Andreas Wachter[3]

Center for Plant Molecular Biology (ZMBP), University of Tübingen, 72076 Tübingen, Germany

ORCID IDs: 0000-0003-3494-2269 (L.H.); 0000-0002-3132-5161 (A.W.).

Alternative splicing (AS) is prevalent in higher eukaryotes, and generation of different AS variants is tightly regulated. Widespread AS occurs in response to altered light conditions and plays a critical role in seedling photomorphogenesis, but despite its frequency and effect on plant development, the functional role of AS remains unknown for most splicing variants. Here, we characterized the light-dependent AS variants of the gene encoding the splicing regulator Ser/Arg-rich protein SR30 in Arabidopsis (*Arabidopsis thaliana*). We demonstrated that the splicing variant *SR30.2*, which is predominantly produced in darkness, is enriched within the nucleus and strongly depleted from ribosomes. Light-induced AS from a downstream 3′ splice site gives rise to *SR30.1*, which is exported to the cytosol and translated, coinciding with SR30 protein accumulation upon seedling illumination. Constitutive expression of SR30.1 and SR30.2 fused to fluorescent proteins revealed their identical subcellular localization in the nucleoplasm and nuclear speckles. Furthermore, expression of either variant shifted splicing of a genomic *SR30* reporter toward *SR30.2*, suggesting that an autoregulatory feedback loop affects *SR30* splicing. We provide evidence that *SR30.2* can be further spliced and, unlike *SR30.2*, the resulting cassette exon variant *SR30.3* is sensitive to nonsense-mediated decay. Our work delivers insight into the complex and compartmentalized RNA processing mechanisms that control the expression of the splicing regulator SR30 in a light-dependent manner.

Maturation of eukaryotic mRNAs involves intricate co- and posttranscriptional RNA processing, which has critical functions in regulating gene expression and diversifying the transcriptome. Among several mechanisms, alternative precursor mRNA splicing (AS) in particular generates many transcript variants by removing distinct intronic regions and joining the resulting exons. Deep analysis of transcriptomes via high-throughput RNA sequencing (RNA-seq) has revealed that a major fraction of all intron-containing genes from higher eukaryotes generates AS variants. In humans, more than 95% of multiexon genes display AS (Pan et al., 2008). The prevalence of AS has also been demonstrated for other eukaryotes including plants (Reddy et al., 2013; Staiger and Brown, 2013), with current estimates of ~61% and ~42% of intron-containing genes giving rise to AS variants in the model plants Arabidopsis (*Arabidopsis thaliana*; Marquez et al., 2012) and *Brachypodium distachyon* (Mandadi and Scholthof, 2015), respectively.

Besides its pivotal role in increasing the coding and regulatory capacity of the transcriptome, AS fine-tunes gene expression by varying the output ratios of splicing variants. The full extent of AS regulation likely exceeds the current estimates, as the production of many transcript variants can be specifically controlled under certain conditions, such as cell and tissue types, developmental stages, and in response to stresses and other environmental factors (Reddy et al., 2013; Staiger and Brown, 2013). The enormous advancement of RNA-seq now allows profiling of this diversity at high depth and spatiotemporal resolution, which is expected to provide important insight into mechanisms and biological functions of AS. For example, comparing the transcriptome patterns between different maize (*Zea mays*) tissues via single molecule long-read sequencing revealed mutually exclusive exon inclusions as the dominant AS type in the endosperm, while regulated intron retention prevailed in other tissues (Wang et al., 2016) and has also been previously described as the most frequent AS type in plants (Filichkin et al., 2010; Marquez et al., 2012; Reddy et al., 2013; Staiger and Brown, 2013).

[1] This work was funded by the German Research Foundation (DFG), with grants WA 2167/4-1, CRC#1101 (C03), and a Heisenberg fellowship (WA 2167/8-1).

[2] These authors contributed equally to the article.

[3] Address correspondence to awachter@zmbp.uni-tuebingen.de.

The author responsible for distribution of materials integral to the findings presented in this article in accordance with the policy described in the Instructions for Authors (www.plantphysiol.org) is: Andreas Wachter (awachter@zmbp.uni-tuebingen.de).

A.W. and L.H. conceived the project; all authors contributed to experimental design; L.H. and T.W. performed the experiments; A.W. supervised the experiments and all authors contributed to data analysis; A.W. wrote the article with contributions from the other authors.

[OPEN] Articles can be viewed without a subscription.
www.plantphysiol.org/cgi/doi/10.1104/pp.17.01260

The generation of AS variants depends on the presence of competing splice sites. Various mechanisms regulate splice site availability and the recruitment of spliceosomal factors as well as splicing regulators to cis-regulatory elements, ultimately defining splice site usage and the AS output. Critical determinants are the regulated formation of mRNA structures (Wachter, 2010, 2014; Wachter et al., 2012; Liu et al., 2015), the recruitment of splicing factors/regulators by components of the transcriptional machinery and associated factors or chromatin marks (Braunschweig et al., 2013), and kinetic coupling between transcription and splicing (Braunschweig et al., 2013; Dolata et al., 2015). Furthermore, the protein level and activity of transacting factors involved in AS decisions is controlled by various means, including expression levels, AS of their own precursor mRNAs (pre-mRNAs), and subcellular protein localization (Wachter et al., 2012; Reddy et al., 2013).

Ser/Arg-rich (SR) proteins and heterogeneous ribonucleoprotein (hnRNP) proteins are two major groups of RNA-binding proteins that are present in animals and plants (Chen and Manley, 2009; Wachter et al., 2012; Reddy et al., 2013). Studies in Arabidopsis demonstrate widespread AS regulatory functions for the hnRNP proteins GLY-RICH PROTEIN7 (GRP7) and GRP8 (Streitner et al., 2012), POLYPYRIMIDINE TRACT BINDING PROTEIN1 (PTB1) and PTB2 (Rühl et al., 2012), RZ-1B/RZ-1C (Wu et al., 2016), and the SR-like protein SR45 (Carvalho et al., 2016). Furthermore, binding motifs required for AS control by SR45 (Day et al., 2012) and the SC35-LIKE33 (SCL33; Thomas et al., 2012) have been identified in single target pre-mRNAs. Recently, transcriptome-wide approaches for profiling interaction sites of RNA binding proteins have been established in plants (Meyer et al., 2017; Xing et al., 2015; Zhang et al., 2015) and are expected to considerably accelerate the discovery of novel AS targets and binding motifs for the large number of potential plant AS regulators.

While it is well established that manifold AS changes are triggered by diverse developmental signals and external cues, few AS events have been functionally characterized in plants. In Arabidopsis, many AS variants are targeted by nonsense-mediated decay (NMD; Kalyna et al., 2012; Drechsel et al., 2013). Coupling of AS and NMD enables quantitative gene control, which is particularly common in the auto- and cross-regulation of splicing regulators, including Arabidopsis SR proteins (Kalyna et al., 2006), GRP7/8 (Staiger et al., 2003; Schöning et al., 2008), and PTBs (Stauffer et al., 2010). Moreover, for some AS events, it has been shown that the splicing variants generate functionally distinct proteins. For example, Kriechbaumer et al. (2012) have demonstrated that tissue-specific AS allows targeting the auxin biosynthetic component YUCCA4 to the endoplasmic reticulum in flowers and to the cytosol in all other examined tissues. Organ-specific AS has also been revealed for the pre-mRNA of the ZINC-INDUCED FACILITATOR-LIKE1 (ZIFL1) transporter (Remy et al., 2013). This AS event causes differential targeting of ZIFL1 to the vacuolar and plasma membrane in root and guard cells, respectively, with specific functions in auxin transport and stomatal movement-dependent drought tolerance. AS of the *PHYTOCHROME INTERACTING FACTOR6* is involved in the regulation of seed germination (Penfield et al., 2010; Rühl et al., 2012).

AS also represents a powerful mechanism to coordinate the expression of sets of genes. Studies in animals demonstrate that specific AS programs underlie certain aspects of neuronal development (Li et al., 2014; Gueroussov et al., 2015; Traunmüller et al., 2016). Furthermore, cell cycle progression is accompanied by periodic AS programs and depends on an SR protein kinase in human cells (Dominguez et al., 2016). In plants, few studies have profiled developmentally controlled AS in a transcriptome-wide manner and at high spatiotemporal resolution. Li et al. (2016) have provided a high-resolution expression map of the Arabidopsis root, covering different cell types and developmental stages. Interestingly, their data also support a role of coordinated AS programs in cell differentiation, while no evidence for AS-mediated cell-type specification has been observed. Furthermore, transcriptome analyses in the course of photomorphogenesis have revealed widespread AS changes within few hours of light exposure of etiolated Arabidopsis seedlings (Shikata et al., 2014; Hartmann et al., 2016). Interestingly, more than 60% of the regulated AS events show a switch from a presumably nonproductive variant in darkness to a probably protein-coding variant in light (Hartmann et al., 2016), thereby allowing to ramp up expression of critical factors. Experimental evidence for such regulation has been provided for the positive light signaling component REDUCED RED-LIGHT RESPONSES IN CRY1CRY2 BACKGROUND1 (Shikata et al., 2012), which displays an AS switch from an NMD target in darkness to a protein-coding transcript variant in light (Hartmann et al., 2016). Furthermore, evidence was provided that photomorphogenesis is promoted by light-dependent AS of *SPA1-RELATED3* (Shikata et al., 2014) due to light-triggered formation of a dominant-negative version of this repressor of photomorphogenesis.

Critical functions of AS in many aspects of plant development and stress responses can also be deduced from the complex phenotypes of splicing regulator mutants (Staiger and Brown, 2013), albeit some of the defects might not result from AS but be linked to other RNA metabolic functions of these factors. Several reports highlight an important role of AS in regulating the plant circadian clock. Accordingly, extensive and temperature-dependent AS has been demonstrated for clock genes from Arabidopsis (James et al., 2012; Filichkin et al., 2015), and mutations in the PROTEIN ARG METHYL TRANSFERASE5 (Sanchez et al., 2010) and the splicing factor SNW/SKI-INTERACTING PROTEIN (Wang et al., 2012) alter circadian rhythms due to mis-splicing of clock genes. Misexpression of SR protein genes results in various changes in plant morphology (Lopato et al., 1999; Kalyna et al., 2003; Ali et al., 2007). Interestingly, several SR and hnRNP protein mutants show altered flowering time (Staiger and Green, 2011; Staiger and Brown, 2013), and a recent report provides evidence for regulation of *FLOWERING LOCUS M* via coupled AS-NMD (Sureshkumar et al., 2016).

The *SR* genes from Arabidopsis are subject to extensive AS regulation, which is modulated in response to hormone treatment and in particular abiotic stresses, such as extreme temperatures, salt stress, and high light (Palusa et al., 2007; Tanabe et al., 2007; Filichkin et al., 2010). Many AS variants derived from the *SR* genes are subject to NMD (Palusa and Reddy, 2010; Kalyna et al., 2012), and differential splicing variant recruitment to polysomes has been observed during development and in response to stresses (Palusa and Reddy, 2015). Interestingly, in the case of the SR-like factor SR45, distinct biological functions of the two AS variants have been demonstrated by complementing a mutant in a splicing variant-specific manner (Zhang and Mount, 2009). While the mutant shows defects in petal development and root growth, complementation with *SR45.1* and *SR45.2* specifically rescues the petal and root phenotype, respectively. However, for most *SR* genes, the specific function of their transcript variants and the impact of AS on gene expression remain unknown.

Here, we functionally characterized light-regulated AS of the *SR30* gene. In dark-grown seedlings, splicing from an alternative upstream 3′ splice site resulted in predominant generation of *SR30.2*, which was enriched in nuclear fractions and depleted in cytosolic fractions. Furthermore, only a minor fraction of *SR30.2* was found to be associated with ribosomes. Light exposure triggered usage of a downstream 3′ splice site, generating *SR30.1*, which is efficiently exported from the nucleus and translated in the cytosol. In line with the distinct subcellular distribution patterns of their mRNAs, the SR30.1 protein accumulated to significant levels, while SR30.2 was not detectable in Arabidopsis plants. Constitutive expression of the two protein isoforms in transient expression systems revealed identical localization patterns of fluorescent protein fusions in the nucleus and similar AS regulation of an *SR30*-based splicing reporter. Besides the major AS variants *SR30.1* and *SR30.2*, we detected the minor cassette exon variant *SR30.3* that is generated by utilizing both alternative 3′ splice sites. *SR30.3* was targeted by NMD, while *SR30.2* was NMD immune. Furthermore, the *SR30.2* cDNA sequence expressed from a transgene could be further spliced to *SR30.3*. Our findings highlight a complex interplay of nuclear and cytosolic processing events in the regulation of *SR30* expression.

RESULTS

Light Induces a Rapid and Transient AS Shift for the Splicing Factor Gene *SR30*

Transcriptome-wide AS profiling of etiolated Arabidopsis seedlings either exposed to different light qualities for 6 h or retained in darkness revealed several hundred AS event changes in response to illumination (Hartmann et al., 2016). Interestingly, the majority of regulated AS events display a switch from a presumably unproductive transcript in darkness to a likely protein-coding variant in light (Hartmann et al., 2016). To understand the regulation and potential impact of this apparently frequent mode of AS shift, AS of *SR30* was functionally characterized. Two major *SR30* variants are generated by AS in etiolated seedlings. *SR30.1* was predominantly produced upon light exposure and encodes the annotated full-length SR30 protein (Fig. 1A; Supplemental Fig. S1). In darkness, *SR30.2* was the major isoform, which results from usage of an upstream 3′ splice site. The additional sequence included in *SR30.2* gives rise to a premature termination codon. Therefore, *SR30.2* contains an extended 3′ untranslated region (UTR) and an intron positioned downstream of the stop codon, features known to be able to trigger NMD in plants (Kerényi et al., 2008).

The levels of these two major *SR30* variants were first measured in etiolated seedlings after various periods of exposure to white light (Fig. 1B). Interestingly, a trend of reciprocal changes in the levels of *SR30.1* and *SR30.2* was already visible after 0.5 h of light exposure. Maximum and minimum levels of *SR30.1* and *SR30.2*, respectively, were reached upon 6 h of white light treatment. Levels of *SR30* splicing variants remained unchanged when seedlings were kept in darkness. These data showed a rapid and transient AS response of *SR30* to white light. Furthermore, reciprocal changes in *SR30.1* and *SR30.2* suggested that the changes occur directly on the level of AS, rather than resulting from light-induced changes in stability of one transcript variant. Illuminating etiolated seedlings with blue (Fig. 1C) and red (Fig. 1D) light also triggered opposite changes in steady state levels of *SR30.1* and *SR30.2*, consistent with the earlier report of similar AS changes in response to different light qualities (Hartmann et al., 2016).

Switching between *SR30* Splicing Variants Regulates Gene Expression

Based on the analysis of transcript features, we expected that *SR30.1* encodes a full-length protein, whereas the presence of a long 3′ UTR as well as a 3′ UTR-located intron in *SR30.2* should trigger NMD. However, analyzing transcript steady state levels in the NMD-impaired mutants *low-beta-amylase1* (*lba1*; Yoine et al., 2006) and *up-frameshift3-1* (*upf3-1*; Hori and Watanabe, 2005) revealed comparable levels of both *SR30.1* and *SR30.2* in the wild type and mutant lines (Fig. 2A). Our analysis also included the minor AS variant *SR30.3*, which we identified by sequencing RT-PCR products from *SR30* and which results from usage of the same alternative 3′ splice site as in *SR30.2* but has an additional splicing event in the region retained in *SR30.2* (Fig. 1A; Supplemental Fig. S1). In contrast to *SR30.2*, *SR30.3* accumulated in the NMD-

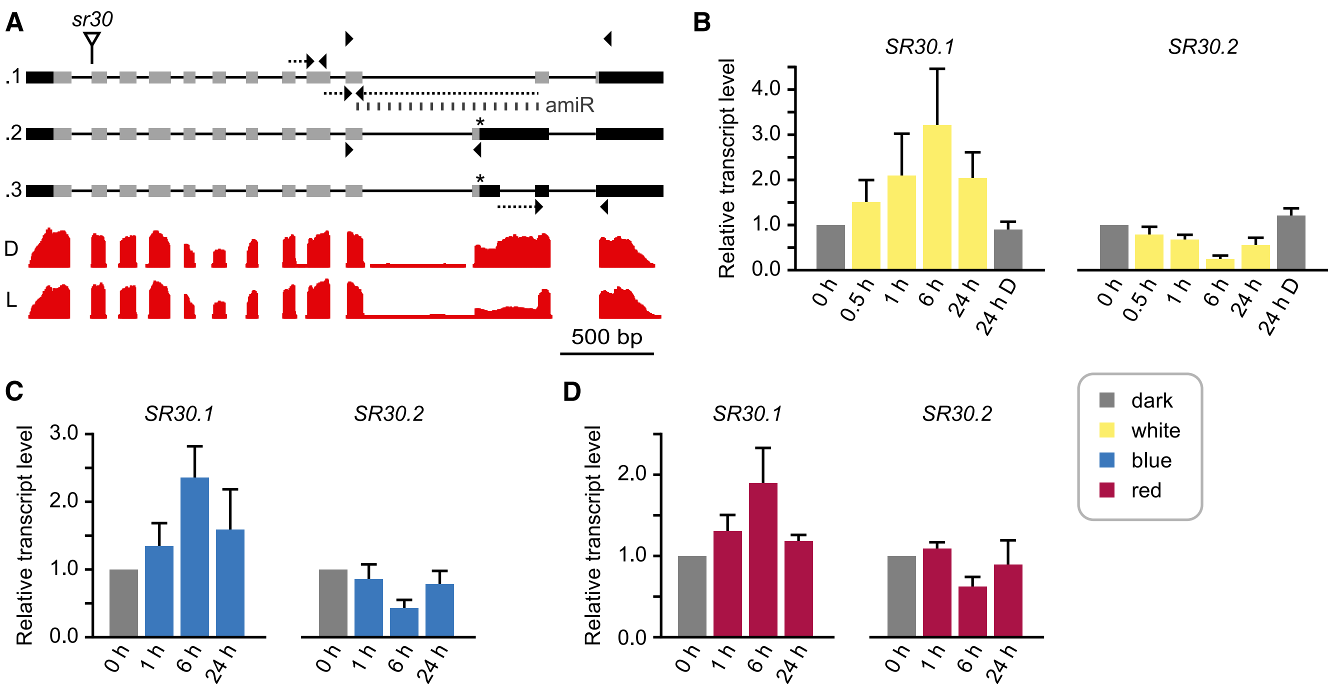

Figure 1. Light exposure triggers opposite changes in levels of major *SR30* splicing variants. A, Gene model of *SR30* including splicing variants analyzed in this work. Primers binding within one exon are shown as arrowheads, whereas arrows with dotted lines indicate primer binding sites spanning splice junctions. The topmost pair are coamplification primers used in downstream analyses, while the primer pair directly above the first variant was used to measure total *SR30* transcripts. Below each variant, the positions of primers used in RT-qPCR for detection of the corresponding splicing variants are indicated. Lines and boxes depict introns and exons, respectively; UTRs and cds are indicated by black and gray shading, respectively. Gray dashed line indicates binding site of artificial microRNA (amiR) spanning a specific splice junction of *SR30.1*. The triangle points at the T-DNA insertion site of *sr30*. Underneath the gene models, representative coverage plots are shown from a previous RNA-seq study (Hartmann et al., 2016) for dark (D) and 6-h white light (L). B to D, Splicing variants were quantified using RT-qPCR in seedlings exposed to white (B), blue (C), or red (D) light for indicated periods. Levels are relative to total *SR30* transcripts and normalized to the 0 h sample. D, Dark; mean values + SD (n = 3–7 for white and n = 3 for blue and red light).

impaired samples relative to the wild type (Fig. 2A). In line with its NMD insensitivity, *SR30.2* displayed a rather high stability, with a half-life of 7.65 h upon transcriptional inhibition (Fig. 2B). Interestingly, *SR30.1* was considerably less stable, displaying a half-life of 1.60 h.

NMD requires translation of its target mRNAs. Thus, a process withholding *SR30.2* from translation could impart immunity to NMD despite the presence of strong NMD-eliciting features. For example, retaining *SR30.2* within the nucleus would prevent its translation and NMD targeting. We therefore examined the distribution of splicing variants in RNA isolated from total samples, cytosol-enriched fractions, and nuclei (Fig. 2, C–E). Purity of the fractions was confirmed by exclusive detection of the nuclear and cytosolic marker proteins histone and UDP-Glc pyrophosphorylase (UGPase), respectively (Fig. 2C). The ratio of *SR30.2/.1* was increased in nuclei compared to total fractions, supporting the theory of impaired nuclear export of *SR30.2* (Fig. 2, D and E). Levels of *SR30.1* and *SR30.2* were also quantified separately in the samples from the fractionation experiment. Compared to the total sample, *SR30.2* was depleted and enriched in the cytosolic and nuclear fraction, respectively (Fig. 2F). We also analyzed ratios of AS variants from *SERRATED LEAVES AND EARLY FLOWERING* (*SEF*) and *RS2Z33*, which have been previously reported to generate AS transcripts that accumulate in the nucleus as a consequence of intron retention (Göhring et al., 2014). The AS ratios of these controls shifted even more toward the longer variant in the nuclear fraction (Fig. 2E), possibly due to more efficient nuclear retention of the intron-retained transcripts compared to *SR30.2*.

To test whether nuclear accumulation of *SR30.2* occurs in a species-specific manner, we transiently expressed a splicing reporter based on the genomic sequence of *SR30* from Arabidopsis in *Nicotiana benthamiana* (see Fig. 5 for reporter diagram and splicing). The reporter gave rise to the same AS variants *SR30.1* and *SR30.2* as in Arabidopsis, and the levels of these transcripts were analyzed in total and fractionated samples. Again, diminished and elevated levels of *SR30.2* were observed in cytosolic and nuclear fractions, respectively (Fig. 2G). When considering both the cytosolic enrichment and nuclear depletion of *SR30.1*,

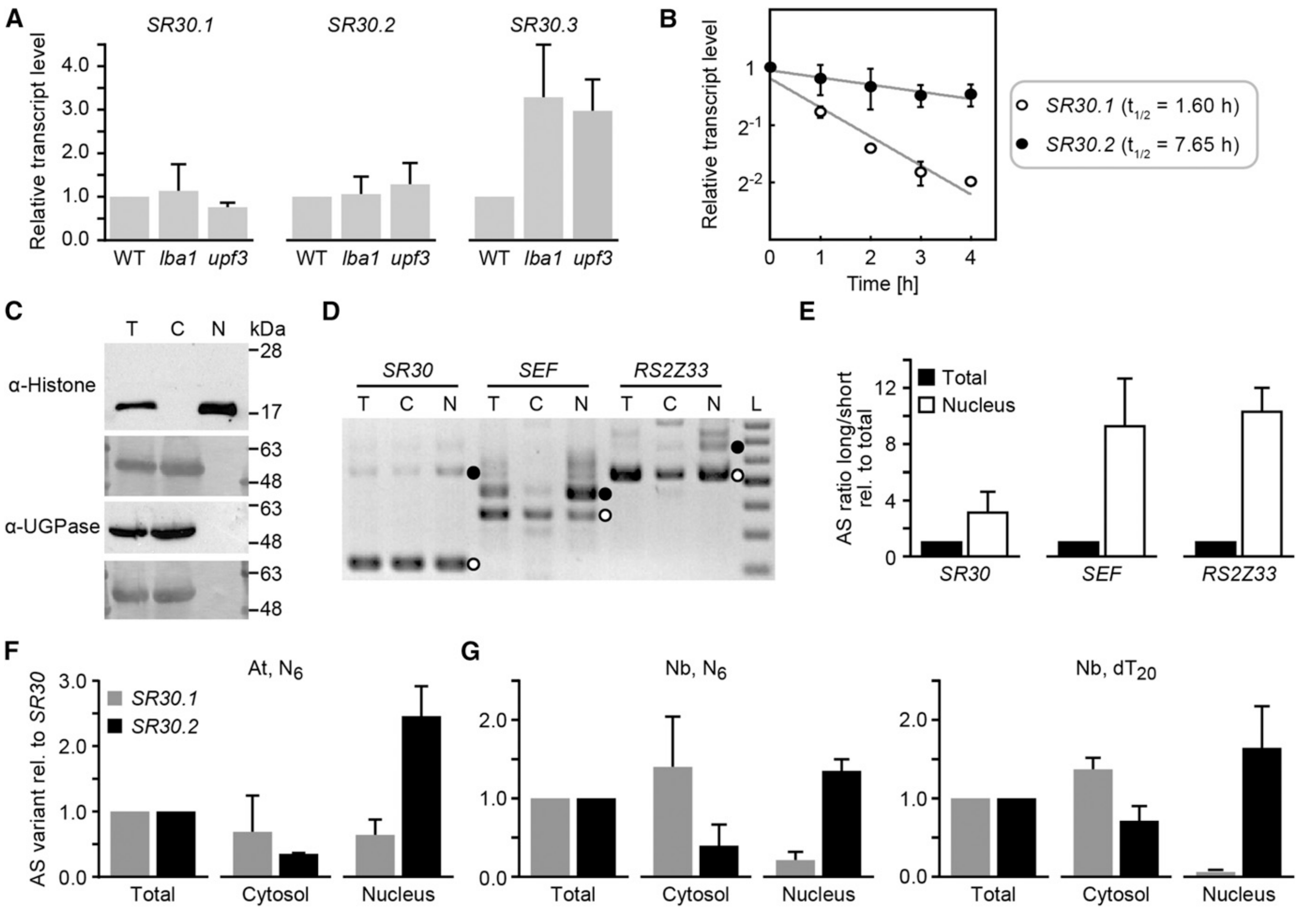

Figure 2. The *SR30.2* variant is relatively stable and enriched in the nucleus. A, *SR30* transcript levels determined via RT-qPCR in 10-d-old green wild-type, *lba1*, or *upf3* seedlings, relative to total *SR30* and the wild type. Mean values + SD; $n = 3$. B, Analysis of *SR30.1* and *SR30.2* RNA stability in 7-d-old Arabidopsis seedlings upon addition of cordycepin. Transcript levels were measured using RT-qPCR and normalized to a stable actin reference. Mean values ± SD are displayed on a $\log_2$ axis; $n = 3$. Half-lives based on exponential regression curves. C, Immunoblot analysis of total (T), cytosolic (C), and nuclear (N) fractions, with histone H3 and UGPase being detected as nuclear and cytosolic markers, respectively. Amidoblack staining shown beneath immunosignals; positions of relevant size marker bands are indicated. D, Coamplification of AS variants for *SR30*, *SEF*, and *RS2Z33* from fractions described in C. Bands corresponding to fragments used for quantitation are marked with white and black dots next to nuclear samples. L, size ladder consisting of DNAs in 100-bp increments from 200 to 800 bp. E, Ratios of long to short AS variants in nuclear fractions relative to total fractions. Mean values + SD; $n = 3$. F and G, Levels of *SR30* AS variants relative to total *SR30* determined via RT-qPCR in indicated fractions from Arabidopsis (At) seedlings (F) and *N. benthamiana* (Nb) leaves expressing an *SR30* reporter (G), using N_6 (left) or dT_{20} (right) for cDNA generation. Mean values + SD; $n = 3$.

the differences in subcellular distribution of the two splicing variants were particularly obvious. We obtained similar results when random hexamer or oligo(dT) primers were used for priming in reverse transcription (Fig. 2G), suggesting that the differential compartmentation of *SR30.1* and *SR30.2* is not explained by the presence of a major fraction of nonpolyadenylated transcripts.

Given the differential subcellular distribution of *SR30* splicing variants and its potential impact on their cellular fate, we analyzed variant levels in mutants defective in nuclear and cytosolic RNA degradation (Supplemental Fig. S2). Mutants with defects in the exosomal core components SUPPRESSOR OF PAS2 2/RRP4 (*sop2-1*) and mRNA TRANSPORT3 (*mtr3*) or a nuclear exosome factor (*hua-enhancer2-4*, *hen2-4*) had an ~2-fold increase in *SR30.1* and *SR30.2* levels; an even stronger accumulation was seen for the cassette exon variant *SR30.3*. In line with the increased levels of the individual splicing variants, total *SR30* transcript levels were also elevated in these mutants. As expected, the *mtr4-1* mutant impaired in nucleolar exosome function showed wild-type-like levels for all *SR30* transcript types. Unchanged steady state levels of all *SR30* transcripts were also observed in a *superkiller* (*ski*) mutant that is defective in a factor contributing to cytoplasmic exosome function. Besides exosome mutants affected in 3′-5′ decay, we also tested a potential role of 5′-3′ exoribonucleases (XRNs) in the degradation of *SR30* transcripts (Supplemental Fig. S2).

A single mutant in the cytoplasmic XRN4 accumulated higher levels of all *SR30* splicing variants. The increase was approximately 2-, 3-, and 4-fold for *SR30.1*, *SR30.2*, and *SR30.3*, respectively. Double mutants impaired in XRN4 and the nucleolar XRN2 or the nucleoplasmic XRN3 showed similar results as the single *xrn4* mutant, suggesting a major role of cytoplasmic but not nuclear 5′-3′ decay. Furthermore, we analyzed the *fiery1-6* (*fry1-6*) mutant, in which the activity of all three XRNs is reduced (Gy et al., 2007). In line with the data from the *xrn* mutants, the variant *SR30.3* strongly overaccumulated in the *fry1-6* seedlings. However, levels of *SR30.1* and *SR30.2* were higher and lower, respectively, in *fry1-6* relative to the *xrn* mutants, possibly due to a change in AS of *SR30* in the *fry1-6* mutant that shows several phenotypical abnormalities. Taken together, our data indicated that both nucleoplasmic 3′-5′ and cytoplasmic 5′-3′ decay contribute to the degradation of all three *SR30* splicing variants. The stronger accumulation of the *SR30.3* variant can be explained by a major impact of RNA turnover on the steady state level of this low abundant splicing variant.

The nuclear enrichment of *SR30.2* and its NMD immunity indicated that at least a substantial fraction of this AS variant did not undergo translation. We directly tested this hypothesis by isolating ribosomes and analyzing the distribution of *SR30* splicing variants in total and ribosomal fractions. Ribosomes were purified via immunoprecipitation from an Arabidopsis transgenic line expressing an epitope-tagged version of the ribosomal protein L18 (RPL18; Zanetti et al., 2005; Mustroph et al., 2013). Successful and specific immunoprecipitation was confirmed by immunoblot detection of the tagged ribosomal protein (Fig. 3A). Coamplification of *SR30.1* and *SR30.2* indicated a weak ribosomal association of *SR30.2* (Fig. 3B), which was confirmed by quantification of the individual splicing variants (Fig. 3C). *SR30.2* was strongly depleted in the ribosomal sample compared to the input, irrespective of the use of random hexamers or oligo(dT) primers for reverse transcription. In contrast, strong ribosomal association was detected for *SR30.1.*

We next investigated whether the small fraction of *SR30.2* transcripts associated with ribosomes gave rise to detectable amounts of a corresponding protein. Constitutive expression of epitope-tagged constructs based on the coding sequences (cds; Fig. 3D) or cDNAs including 5′ and 3′ UTRs (Fig. 3E) of *SR30.1* and *SR30.2* in *N. benthamiana* resulted in robust protein accumulation for SR30.1. In contrast, no or much weaker protein signals were detected upon expression of the constructs based on *SR30.2*. *SR30.1* and *SR30.2* are predicted to encode proteins of 30.4 and 29.1 kDa, respectively, and the triple HA tag is expected to increase protein size by ~3 kDa. The expression of both constructs resulted in immunosignals of similar M_r slightly above 40 kDa. Immunoblot detection using an affinity-purified antibody that was raised against the recombinant full-length SR30.2 protein confirmed the results obtained with the tag-specific antibody (Fig. 3E).

Considering that the expression via infiltration assays of *N. benthamiana* leaves represents an artificial and transient system, we also tested SR30 protein accumulation in Arabidopsis wild-type and stably transformed lines. Immunoprecipitation followed by immunoblot analysis with the SR30 antibody resulted in a double band of ~40 kDa for wild-type Arabidopsis seedlings (Fig. 3, F and G). The lower signal was absent in a transgenic line expressing an artificial microRNA (amiR) directed against *SR30.1* (Fig. 3G; Supplemental Table S1) as well as in the T-DNA insertion line *sr30* (Supplemental Fig. S3, A–C), which was expected to be impaired in the expression of any SR30 protein. Accordingly, the lower signal of the double band in wild-type plants can be assigned to the SR30 protein. Furthermore, SR30 protein detection in transgenic lines expressing tagged versions of the cDNAs from *SR30.1* and *SR30.2* (Supplemental Table S1) resulted in an additional, upward shifted signal for *SR30.1* (Fig. 3F). This signal was also detectable using a tag-specific antibody. In contrast, no construct-specific protein signal was observed in the case of *SR30.2* overexpression, in line with our finding of low or undetectable accumulation of this protein upon transient expression. The upper signal of the double band detected in wild-type and transgenic seedlings may represent an unspecific signal or cross-detection of a related SR protein. Given the pronounced AS shift of *SR30* during photomorphogenesis, we also analyzed SR30 protein levels in etiolated seedlings exposed to light for different periods as well as in light-grown seedlings. The specific SR30 signal was weakest in etiolated seedlings and became stronger with the duration of light exposure (Supplemental Fig. S3C), in agreement with a light-induced switch to the protein-coding variant *SR30.1*. Taken together, our data indicated that light-mediated AS of *SR30* mainly functions in quantitative gene control, whereas no evidence for significant accumulation of the alternative protein SR30.2 in wild-type samples was found.

Proteins Encoded by the *SR30* Variants Show Comparable Nuclear Localization and Splicing Regulatory Functions

Immunological detection of the proteins generated upon transgenic expression of the *SR30* variants revealed that *SR30.2* results in substantially weaker signals than *SR30.1*, irrespective of the presence or absence of the UTRs. The proteins encoded by the two major AS variants of *SR30* differ only in their C termini. Due to upstream 3′ splice site usage, *SR30.2* possibly encodes a protein that is 12 amino acids shorter than SR30.1 and that ends with a specific sequence of 10 amino acids. To test if AS of *SR30* enables not only quantitative control of gene expression but can also give rise to potentially functionally distinct proteins under any condition, we first analyzed the subcellular localization of both protein variants. Reporter constructs containing fusions of the cds from *SR30.1* or *SR30.2* and yellow or cyan fluorescent protein were transiently expressed in Arabidopsis protoplasts, followed

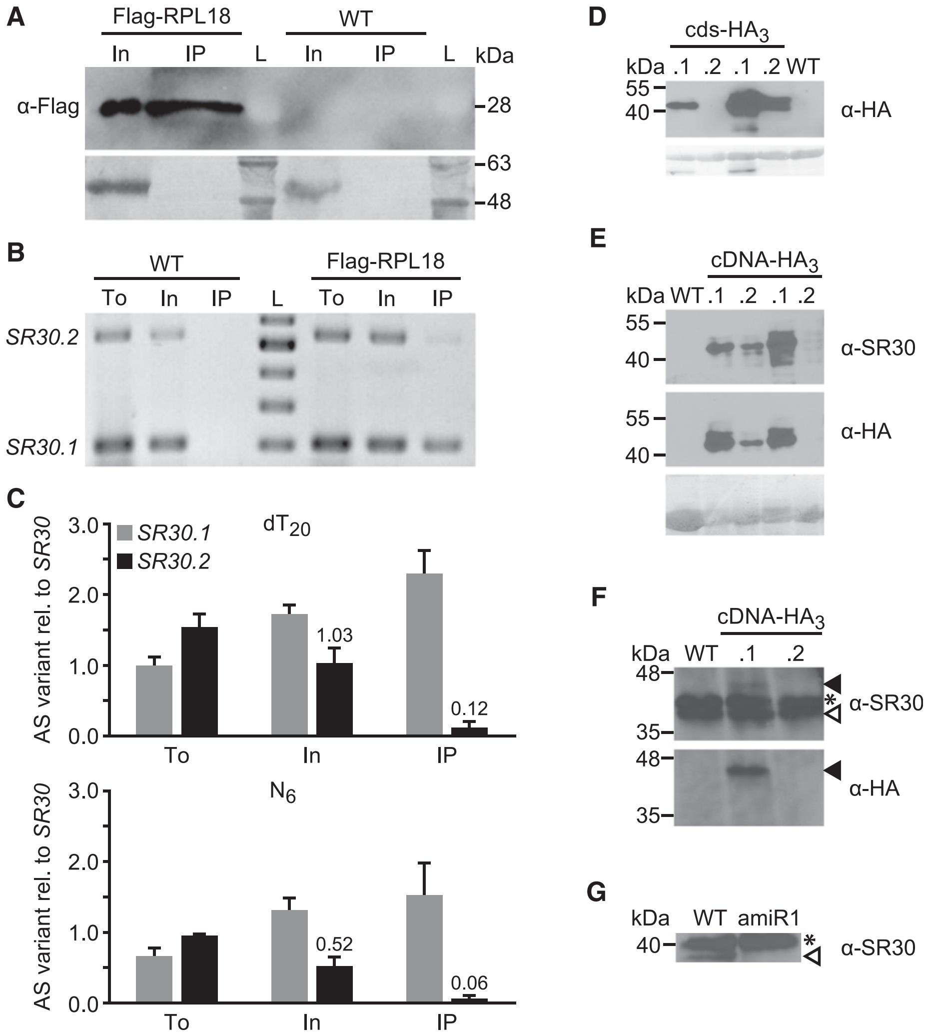

Figure 3. Splicing to *SR30.2* results in diminished protein production. A, Immunoblot detection of Flag-tagged RPL18 in input (In) and immunoprecipitation (IP) fractions of 10-d-old green Arabidopsis seedlings from indicated genotypes. Twenty micrograms of total protein of In (~0.1% of In) and 6% of IP sample was loaded. L, ladder containing proteins of indicated sizes. Upper and lower panels depict immune signal and amidoblack staining, respectively. B, RT-PCR coamplification of *SR30.1*/*.2* from total RNA preparation (To; standard RNA extraction directly from freshly frozen material) and samples described in A. L, size ladder consisting of DNAs in 100-bp increments from 200 to 600 bp. C, Levels of *SR30.1* and *SR30.2* were determined via RT-qPCR in samples described before and are depicted relative to total *SR30* transcripts and normalized to a total sample from the wild type. Reverse transcription of RNAs performed with dT_{20} (top) or N_6 (bottom) primers. Mean values + SD; $n = 3$. Values for *SR30.2* in relevant In and IP fractions are provided. D and E, Immunoblot detection of HA-tagged SR30.1 and SR30.2 in *N. benthamiana* upon transient expression of constructs based on the cds (D) or the cDNAs with 5′ and 3′ UTRs (E). Each sample pair came from corresponding leaf halves. WT, Noninfiltrated leaf. Fifteen micrograms of total protein each (D) or fresh weight equivalents (E) were loaded; lower panels show amidoblack staining as the loading control. F and G, Immunoblot analysis upon immunoprecipitation with α-SR30 from 10-d-old green wild-type or transgenic Arabidopsis seedlings, expressing indicated cDNA-HA_3 constructs (F) or an amiR construct targeting *SR30.1* (G). Fresh weight equivalents were loaded; cross-detection band (asterisk) serves as the loading control. Open arrowheads indicate endogenous SR30, and closed arrowheads in (F) mark tagged SR30.1.

by in vivo imaging. Note that UTR-free constructs were used for constitutive expression in an artificial and transient assay and that inspection of fluorescence in individual protoplasts does not allow a quantitative comparison of the accumulation for the two SR30 variants. Both SR30.1-YFP and SR30.2-YFP were detectable and colocalized with the marker construct NLS-DsRED in the nucleus (Fig. 4A; Supplemental Fig. S4A). Colocalization studies of SR30.1 and SR30.2 reporter fusions showed completely overlapping signal patterns (Fig. 4, B–D). Within the nucleus, the fusion proteins generally localized in the nucleoplasm, while they were absent from the nucleoli. In some protoplasts, both fusion proteins also accumulated in nuclear speckles (Fig. 4D). To test if the presence of a fluorescent protein tag in the localization constructs affected the accumulation of the corresponding

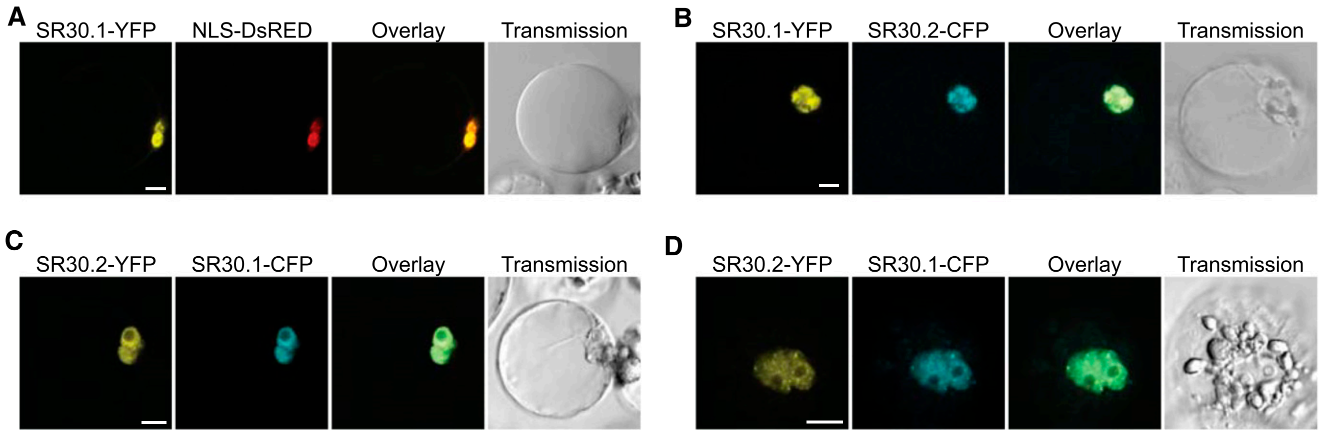

Figure 4. Fluorescent protein fusions of SR30.1 and SR30.2 both localize to the nucleus in Arabidopsis protoplasts. A, A construct containing the cds of *SR30.1* fused to *YFP* was transiently coexpressed with the nuclear marker NLS-DsRED in Arabidopsis protoplasts, followed by imaging using confocal microscopy. B and C, Colocalization of SR30.1 and SR30.2 fusions. D, Colocalization of SR30.2-YFP and SR30.1-CFP in the nucleoplasm and speckles. Bars = 10 μm in all panels.

fusion proteins and to be able to compare their levels quantitatively, we transiently expressed the reporter fusions in *N. benthamiana*, followed by immunoblot analysis. In agreement with the previous immunoblots, the fusions containing SR30.1 resulted in strong protein signals, whereas the SR30.2 fusions were not detected or were barely detectable (Supplemental Fig. S4B). SR30.1-Y/CFP was detected as two bands with a size of ~70 kDa. This corresponded to a size shift of approximately 10 kDa above the theoretical size, as we observed for the other SR30 immunosignals. Taken together, our data suggested that *SR30.2* resulted in considerably lower protein accumulation than *SR30.1*, most likely as a consequence of the nuclear retention of *SR30.2*. While we cannot exclude that other parameters, such as the degree of protein extractability, contributed to the differences in strength of the immunosignals between SR30.1 and SR30.2, the very small fraction of *SR30.2* associated with ribosomes suggested that its low level of translation was the main cause for our observation.

Previous work indicated that SR30 can regulate AS of its own pre-mRNA, as overexpressing *SR30* results in an altered AS output for the endogenous *SR30* locus (Lopato et al., 1999). However, effects of the proteins potentially encoded by the two AS variants of *SR30* have not been compared. To allow a quantitative comparison, a splicing reporter based on the genomic sequence of *SR30* and containing a tag sequence for specific detection (Fig. 5A) was coexpressed with cds constructs of *SR30.1* and *SR30.2*. Interestingly, both SR30.1 and SR30.2 shifted reporter splicing toward the *SR30.2* transcript version (Fig. 5B). Quantitation of the data revealed that the two SR30 variants displayed a comparable splicing regulatory activity (Fig. 5C). In summary, enforcing the expression of the two protein variants using a strong constitutive promoter and omitting the UTRs did not provide evidence that AS of *SR30* can give rise to functionally distinct proteins.

The *SR30.2* Transcript Can Be Further Spliced

A substantial fraction of *SR30.2* transcripts was found in the nucleus, where these transcripts may be subject to further processing including degradation. Interestingly, light-induced AS of *SR30* not only led to an altered ratio of *SR30.1*/*SR30.2*, but also caused significant changes for several cassette exon events in the

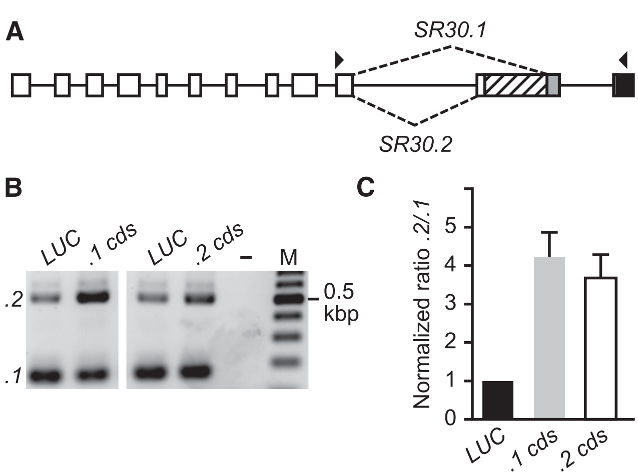

Figure 5. Both SR30.1 and SR30.2 can alter splicing of the *SR30* pre-mRNA. A, Gene model of the reporter used for the splicing assay. Exons are shown as boxes and introns as lines. White, cds; hatched, 3′ UTR in *SR30.2*; gray, cds in *SR30.1* and 3′ UTR in *SR30.2*; black, HA-tag. Arrowheads indicate binding positions of primers for coamplification of resulting splicing variants. With the exception of the HA-tag, model is drawn to scale. B, RT-PCR products upon coamplification of splicing variants *SR30.1* and *SR30.2* from the reporter coexpressed with a control protein (luciferase [LUC]) or the cds of *SR30.1* and *SR30.2*. Shown is representative agarose gel including a no template control (−) and DNA size ladder (M) with 100-bp increments. C, Ratio quantification using a Bioanalyzer for splicing variants displayed in B and normalized to the control (LUC). Mean values + SE; *n* = 14 to 15.

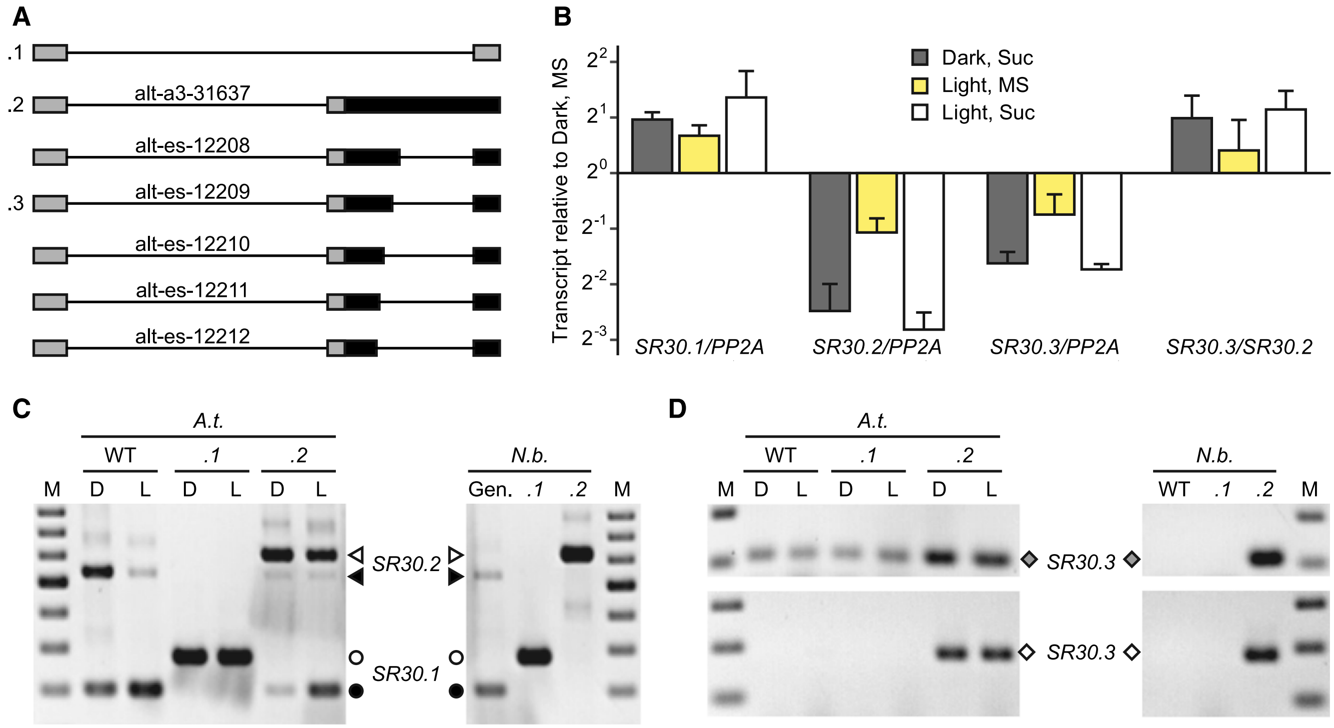

Figure 6. *SR30.2* can be further spliced to *SR30.3*. A, Partial models of *SR30* alternative splicing variants that were previously identified (Hartmann et al., 2016) to be significantly altered relative to *SR30.1* upon light exposure of etiolated seedlings. Lines and boxes correspond to introns and exons, respectively. Gray and black fills indicate coding sequence and 3′ UTR, respectively; AS event identifiers from previous study (Hartmann et al., 2016) are provided. B, Levels of *SR30* splicing variants relative to reference *PP2A* and ratio *SR30.3/SR30.2* were determined using RT-qPCR from *lba1* seedlings grown for 6 d in darkness and then retained in darkness or exposed for 6 h to white light in liquid control medium (MS) or medium containing 2% Suc. Data normalized to corresponding values from seedlings kept in dark and MS. Mean values + SD; $n = 3$ for sugar and light treatments and $n = 2$ for dark/MS controls. C, RT-PCR products upon coamplification of *SR30.1* (circles) and *SR30.2* (arrowheads) from Arabidopsis (A.t.) seedlings grown for 6 d in dark (D) or under long-day conditions (L) or *N. benthamiana* (N.b.) leaves transformed with *SR30* constructs. Transformation results in constitutive expression of cDNA constructs (*.1* and *.2*) based on the corresponding Arabidopsis *SR30* variants or the genomic Arabidopsis *SR30* sequence (Gen.). Black symbols indicate positions of products corresponding to endogenous splicing variants, and white symbols point at transgene-derived products that are size-shifted due to the presence of a tag. Size marker (M) consists of DNAs in 100-bp increments, with the lowest band representing 200 bp. D, RT-PCR products upon amplification of *SR30.3* (indicated by diamonds), either from the endogenous locus and transgene (upper gel) or specifically from the transgene (lower gel). Samples as in C, with added nontransformed wild-type control for *N. benthamiana*. Size marker in 100-bp increments; top bands correspond to 200 and 300 bp in upper and lower gels, respectively.

same region (Fig. 6A; data from Hartmann et al., 2016). The cassette exons result from two splicing events using both alternative 3′ splice sites, whereas for *SR30.1* and *SR30.2* only the downstream and upstream 3′ splice site, respectively, are used. The five cassette exon variants include *SR30.3* and differ only in their 5′ splice site within the region that is retained in *SR30.2* and intronic for *SR30.1* (Fig. 6A; Supplemental Fig. S5). The corresponding cassette exons are 165, 147, 127, 117, and 112 bp in size. Three of the cassette exon events (alt-es-12209/12210/12211) have been previously identified as being regulated by NMD (Drechsel et al., 2013). NMD targeting of *SR30.3* (alt-es-12209) was confirmed in this study (Fig. 2A). Based on the coverage plots from the RNA-seq data and the absence of bands corresponding to the cassette exon variants in RT-PCR reactions coamplifying *SR30.1* and *SR30.2*, we concluded that the steady state levels of the cassette exon variants were relatively low. Their low abundance can result from minor usage of the corresponding splice sites and/or high transcript turnover, in line with NMD targeting of *SR30.3* and its strong overaccumulation in RNA degradation mutants. Remarkably, further splicing of *SR30.2* might produce the cassette exon variants and thereby induce nuclear export and cytoplasmic decay of these transcripts. In support of such a route for generating the cassette exon variants, no splicing variants were observed that retained the intron upstream of the cassette exons or were derived from using alternative 5′ or 3′ splice sites in this upstream region.

To investigate how AS of *SR30* affects the generation of the various splicing variants, their levels were analyzed in dark-grown seedlings as well as upon light and/or sugar treatment, based on the previous observation that both signals trigger AS for *SR30* and other genes (Hartmann et al., 2016). We used seedlings of wild type and the NMD-impaired mutant *lba1*, in which the NMD target *SR30.3* overaccumulated relative to the wild type, while levels of *SR30.1* and *SR30.2* were not affected (Fig. 2A). In line with our previous observations (Hartmann et al., 2016), both light and sugar exposure caused an increase of *SR30.1* and a concomitant reduction of *SR30.2* in *lba1* seedlings (Fig. 6B; Supplemental Fig. S6A). *SR30.3* was used as a proxy for the cassette exon variants, as measuring them collectively by RT-qPCR without detecting *SR30.2* is not possible. Interestingly, levels of *SR30.3* were also reduced in sugar- and light-treated seedlings (Fig. 6B). The reduction in *SR30.3* was less pronounced than for *SR30.2*, as also reflected by an increased ratio of *SR30.3*/*SR30.2* upon sugar and light treatment (Fig. 6B). The increased ratio of *SR30.3*/*SR30.2* in sugar-/light-treated samples may result from further splicing of *SR30.2* to the cassette exon variants; this AS ratio change is in line with the activation of the downstream 3′ splice site, which is also used for splicing of the pre-mRNA to *SR30.1* under these conditions. As an alternative to the generation of the cassette exon variants from the mature *SR30.2* mRNA, these transcripts may also originate directly from splicing of the pre-mRNA. Similar light- and sugar-induced changes in the levels of the individual *SR30* variants were observed for wild-type seedlings (Supplemental Fig. S6B). However, changes in the *SR30.3*/*SR30.2* ratios were less pronounced in the wild type compared to *lba1* seedlings, possibly due to different turnover rates of *SR30.3*.

We next tested whether *SR30.3* can be spliced from a cDNA corresponding to the *SR30.2* sequence or if the authentic pre-mRNA context is required. Therefore, *SR30* AS patterns were determined in Arabidopsis seedlings and infiltrated *N. benthamiana* leaves expressing constructs based on *SR30.1* or *SR30.2.* Coamplification with primers spanning the alternatively spliced region of *SR30* detected endogenous *SR30.1* and *SR30.2* in wild-type Arabidopsis seedlings, with the light-dependent differences in the ratios as described before (Fig. 6C, left). In Arabidopsis seedlings transformed with 35S promoter-driven constructs based on the *SR30.1* or *SR30.2* cDNAs, the main signal corresponded to the respective transgene, independent of the light condition. This observation further substantiated the conclusion that light-dependent changes in the levels of *SR30* transcript variants resulted from AS and not altered transcript turnover rates. The products derived from the transgene and the endogenous locus could be distinguished by their size difference; due to the presence of a tag in the constructs, the corresponding RT-PCR products were larger than those derived from the endogenous *SR30* locus. In the lines overexpressing *SR30.2*, the endogenous *SR30.1* and its light induction was still visible, while endogenous *SR30.2* was not detected in the lines overproducing *SR30.1* (Fig. 6C, left). This is likely due to the fact that *SR30.1* and *SR30.2* accumulated to different extents. In *N. benthamiana* leaves transiently expressing a construct based on the genomic sequence of *SR30* from Arabidopsis (Fig. 6C, right), both major *SR30* splicing variants were detected. In contrast, leaves expressing the cDNA constructs allowed only detection of the respective variants. We next used these samples to examine whether the *SR30.2* cDNA can be further processed to *SR30.3*. Using a primer combination that can detect *SR30.3* produced both from the endogenous *SR30* locus and the transgene (Fig. 6D, upper panel) resulted in detection of this variant in all Arabidopsis samples and *N. benthamiana* leaves expressing *SR30.2*. Furthermore, the level of *SR30.3* was strongly increased upon *SR30.2* overexpression, while *SR30.1* overexpression had no effect on the accumulation of the cassette exon variant in the stably transformed Arabidopsis lines (Supplemental Fig. S6C). To support direct processing of *SR30.2* to *SR30.3*, we used a tag-specific primer in combination with an *SR30.3*-specific primer. Indeed, *SR30.3* production from the transgene was found in all samples expressing the *SR30.2* construct (Fig. 6D, lower panel). This splicing event from *SR30.2* to *SR30.3* is expected to trigger nuclear export of the transcript, followed by its translation and degradation via NMD, which may represent a major route of its turnover. Additional work is needed to test if our finding of further splicing of a transgene-derived *SR30.2* variant also applies to generation of the corresponding *SR30* transcripts from the endogenous locus. Interestingly, inspection of AS patterns for several other *SR* genes revealed the occurrence of similar AS events within long introns as for *SR30*, suggesting that related splicing mechanisms may be more common (Supplemental Fig. S7).

DISCUSSION

Regulation of *SR30* Expression via Alternative RNA Processing in the Nucleus and Cytosol

We have demonstrated in this study that light-regulated AS controls expression of *SR30* by creating splicing variants that show distinct subcellular distribution patterns and are degraded via different mechanisms (Fig. 7). In the presence of light, usage of the downstream 3′ splice site generates *SR30.1*, which is exported to the cytosol and translated into the corresponding splicing regulator. In darkness, splicing from the upstream 3′ splice site produces *SR30.2*, which is enriched in the nucleus and depleted from the cytosolic fraction. The nuclear enrichment of *SR30.2* is in line with its weak ribosomal association and NMD immunity, despite the presence of a premature termination codon and long 3′ UTR, both of which are NMD-triggering features. The nuclear enrichment of *SR30.2* can result from either impaired export of this splicing variant into the cytoplasm or accelerated turnover in the cytoplasm. Given that *SR30.2* accumulates only slightly stronger than *SR30.1* in cytoplasmic RNA decay mutants and that *SR30.2* is significantly more stable than *SR30.1*, we think that impaired nuclear export of *SR30.2* is mainly responsible for our observations. Additionally, the minor variant *SR30.3* retaining a cassette exon within

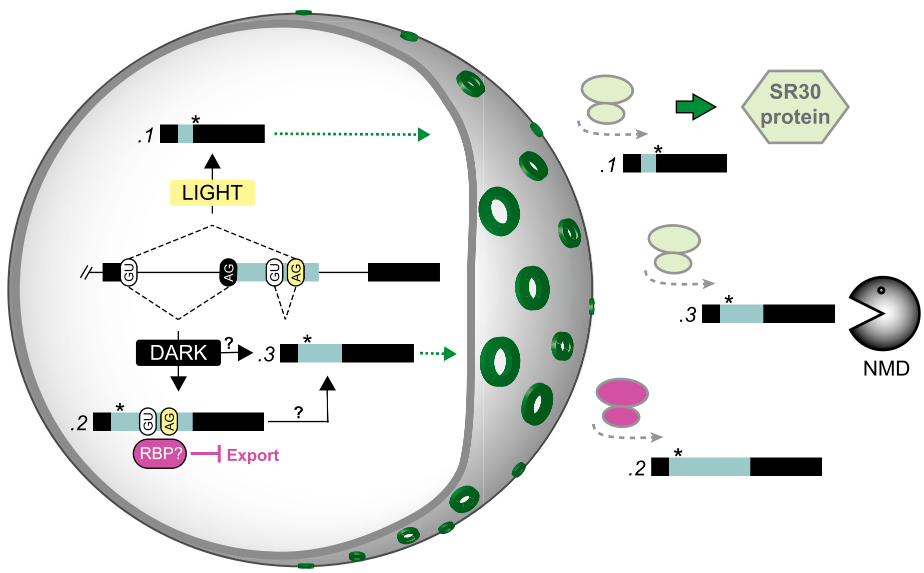

Figure 7. Model of *SR30* regulation via AS and downstream processes. Boxes and lines depict exons and introns, respectively, of *SR30* transcripts, for which only the part from the exon upstream of the alternatively spliced region to the 3′ end of the mRNAs is displayed. Asterisks depict positions of first in-frame translational stop codons for each mRNA. RBP indicates a putative RNA-binding protein. Dark-gray shape represents nuclear envelope with pores for export (green rings). Active translation is indicated by light-green ribosome symbols. Magenta indicates impairment of the corresponding process.

the alternatively spliced region has been detected. Based on the currently available data, generation of *SR30.3* by splicing of the primary pre-mRNA as well as consecutive splicing of the *SR30.2* mRNA seem plausible (see discussion below). NMD targeting of *SR30.3* and, according to published RNA-seq data (Drechsel et al., 2013), other cassette exon variants of *SR30* implies that these mRNAs are exported from the nucleus and translated. Based on our results, we propose that regulated AS of *SR30* allows rapid adjustment of the expression of this splicing regulator to ambient light conditions.

Our findings reveal an unexpected complexity of AS variant formation and downstream regulatory processes. The observation of nuclear enrichment of a splicing variant resulting from alternative 3′ splice site usage in the *SR30* pre-mRNA suggests that many other AS events may affect nuclear export of the corresponding splicing variants. A previous study reported nuclear accumulation of intron-retained transcripts (Göhring et al., 2014); however, our data show that splicing from an alternative 3′ splice site can similarly affect the subcellular distribution of mRNAs. Intron retention and alternative 3′ splice site usage have been described as the most common types of AS in plants, with varying frequencies in different studies (Marquez et al., 2012; Rühl et al., 2012; Hartmann et al., 2016). Furthermore, it seems likely that other AS types, such as splicing from alternative 5′ splice sites, can also prevent efficient nuclear export of the corresponding splicing variants. Nuclear enrichment of certain AS variants has also been observed in a previous study comparing the transcript profiles in libraries constructed from Arabidopsis whole cells, nuclei, and nucleoli (Kim et al., 2009). Interestingly, it was reported that many of these AS variants are enriched in the nucleolus compared to the nucleoplasm (Kim et al., 2009). In contrast to *SR30.2*, however, several of the nucleolus-enriched AS variants that were further analyzed by Kim et al. (2009) showed NMD targeting. Thus, specific regulation of mRNA transport within and export from the nucleus must occur. One possible scenario is that a particular RNA-binding protein associated with a completely or partially retained intron of a splicing variant prevents its nuclear export (Fig. 7). The nuclear retained transcripts may then be subjected to degradation in this compartment. Alternatively, removal of the corresponding protein factor, e.g. as a result of further processing, may enable export of the mRNA into the cytosol at a later point.

Possible Alternative Routes for the Generation of the *SR30.3* Variant

We have shown that a transgene-derived cDNA corresponding to the fully spliced *SR30.2* sequence can be further spliced to *SR30.3*. Several observations are in line with the hypothesis that endogenous *SR30.3* and the other cassette exon variants can also be generated by consecutive splicing of *SR30.2*, as opposed to independent removal of the two introns flanking the cassette exons from the pre-mRNA. First, no splicing variants have been identified in which the intron downstream of the cassette exon has been removed while the upstream intron is still present. Second, for all cassette exon variants, the splice sites used for removal of the upstream intron conform to the sites specifying *SR30.2*, while various 5′ splice sites are used for splicing of the intron downstream of the cassette exon. Regulation of AS in this region can be explained by the presence of two competing 3′ splice sites. In darkness, the upstream 3′ splice site is preferred, resulting in formation of *SR30.2*. Light and sugar signals trigger formation of *SR30.1* by activating the downstream 3′ splice site, e.g. by binding of a negative or positive splicing regulator, respectively, near the up- and downstream 3′ splice site. Due to usage of the identical 5′ splice site, generation of the two major splicing forms *SR30.1* and *SR30.2* is mutually exclusive. However, *SR30.2* still contains a substantial portion of the sequence that is intronic for *SR30.1*, including the 3′ splice site. Therefore, in a second step, splicing of *SR30.2* to the cassette exon variants could occur, independent of the other introns. Such a consecutive splicing mechanism giving rise to the *SR30* cassette exon variants would be reminiscent of recursive splicing that was first described for the *ULTRABITHORAX* gene in *Drosophila melanogaster* (Hatton et al., 1998). In this example, a large intron is not spliced as a single unit, but in a sequential manner by recreating 5′ splice sites after splicing. Recently, further examples of recursive splicing events, involving generation of zero nucleotide exons, have been described for *D. melanogaster* (Duff et al., 2015). Identification of recursive splicing in vertebrate genes (Sibley et al., 2015) demonstrated that this mechanism is not restricted to *D. melanogaster*. Interestingly, all of the recursive splicing events found in human can result in cassette exon inclusion (Cook-Andersen and Wilkinson, 2015; Sibley et al., 2015), equivalent to the proposed consecutive splicing events resulting in *SR30.3*. In the first step, the intron upstream of the cassette exon is spliced out. In the second step, splicing from a 5′ splice site either at the start of the cassette exon or downstream of it results in removal and inclusion of the cassette exon, respectively. Like *SR30.3*, most of the cassette exon variants resulting from recursive splicing in vertebrate genes are targeted by NMD (Sibley et al., 2015). Interestingly, the regulated intron in *SR30* and the corresponding introns from other *SR* genes showing *SR30*-like AS patterns are exceptionally long, with 942 nucleotides for *SR30* and ranging from 765 to 1100 nucleotides for the other cases (Supplemental Fig. S7). In contrast, the average intron length in Arabidopsis is only 165 nucleotides according to TAIR10 (Lamesch et al., 2012). Accordingly, these long introns may have specifically evolved to allow gene regulation via mechanisms related to those proposed in this work. Further work is needed to be able to distinguish between the alternative routes of cassette exon variant formation for these *SR* genes, involving either activation of multiple AS sites on the pre-mRNA or consecutive splicing of mRNAs. Given the low steady state levels of *SR30.3* and the other cassette exon variants, its relevance for the regulation of *SR30* expression also remains open. In light of NMD targeting of these splicing variants and the strong accumulation of *SR30.3* in exosome and *xrn* mutants, however, it is possible that a substantial fraction of all *SR30* pre-mRNAs is spliced to the cassette exon isoforms, which do not accumulate due to rapid turnover.

In case the *SR30* pre-mRNA is spliced consecutively, the timing of the two splicing events will be of particular interest. Previous work indicated that posttranscriptional splicing can be activated on demand. Boothby et al. (2013) demonstrated that splicing of retained introns allows regulation of translation during gametophyte development in the fern *Marsilea vestita*. Our AS analysis revealed a slight increase in the ratio *SR30.3*/*SR30.2* in light- and sugar-treated seedlings compared to dark controls. This AS ratio change and the increased formation of *SR30.1* are in line with an activation of the downstream 3′ splice site upon light and sugar availability. Moreover, *SR30.2* may not only function in gene regulation by being withheld from translation, but could also fulfill specific functions in the nucleus. For example, this splicing variant may sequester or assemble splicing regulators and thereby affect the AS outcome of other pre-mRNAs, similar to what has been described for a long noncoding RNA in Arabidopsis. This long noncoding RNA can interact with nuclear speckle RNA-binding proteins and thereby alter the AS outcome of their target pre-mRNAs (Bardou et al., 2014). Further splicing of *SR30.2* may also compete with nuclear decay of this splicing variant. Precedence for such a mechanism comes from the identification of exosome mutants as suppressors of a splicing-defective allele of *PASTICCINO2* (*PAS2*; Hématy et al., 2016). The suppressor mutants *sop1*, *sop2*, and *sop3* displayed an accumulation of an intron-retaining *pas2-1* isoform, which probably allowed increased splicing to a variant complementing the *pas2-1* phenotype. Our analysis of *SR30* transcript levels in exosome and *xrn* mutants indicated that both nucleoplasmic 3′-5′ and cytoplasmic 5′-3′ decay contributed to the turnover of all three variants. Accordingly, the two pathways may compensate for a defect in one of their components in the corresponding mutants. The observation of cytosolic and nucleoplasmic turnover for *SR30.2* and *SR30.3*, respectively, is of particular interest, as it points to the existence of additional mechanisms limiting their accumulation. Specifically, some *SR30.3* transcripts are already targeted for degradation in the nucleus before they can be exported to the cytoplasm, and *SR30.2* mRNAs escaping the nucleus are subjected to XRN4-mediated decay in the cytoplasm. However, given that *SR30.2* accumulates only slightly more than *SR30.1* in the *xrn* mutants and as *SR30.2* shows a much higher stability than *SR30.1*, we think it is unlikely that alternative turnover rates alone can explain the differential subcellular distribution patterns of the two splicing variants. The NMD immunity of *SR30.2* also is in line with our model that most of this transcript variant is not available for translation in the cytoplasm, albeit additional mechanisms suppressing translation of this splicing variant may exist.

Distinct Subcellular Localization of *SR30* mRNA Variants

Key to the specific fates of the *SR30* splicing variants is their distinct subcellular distribution. Regulated localization of RNAs within the cell is found from bacteria to higher eukaryotes and emerging evidence suggests its frequent occurrence (Chin and Lécuyer, 2017). A first direct link between mRNA localization and splicing was provided in *D. melanogaster* for the

OSKAR mRNA, which needs to contain the first intron of the pre-mRNA and be spliced in it, in order to correctly localize to the posterior pole of the oocyte cytoplasm. Subsequent studies identified the molecular mechanisms of this splicing requirement, including deposition of the exon junction complex (Newmark and Boswell, 1994; Mohr et al., 2001; van Eeden et al., 2001; Hachet and Ephrussi, 2004; Palacios et al., 2004) and formation of an RNA structural element defining the localization of the *OSKAR* mRNA (Ghosh et al., 2012). Furthermore, evidence has been provided that AS is used to achieve distinct subcellular localization of the mature mRNA variants (Chin and Lécuyer, 2017). However, with the exception of the study by Göhring et al. (2014), most of our current knowledge on splicing-dependent RNA localization is based on studies in animal systems. Our finding of nuclear retention of *SR30.2* provides a good starting point for further investigating the molecular basis of the subcellular localization of this splicing variant, e.g. by searching for protein factors that are specifically associated with *SR30.2* and not the other *SR30* AS variants or by mapping the critical RNA region.

While our data indicated that the major portion of *SR30.2* is retained within the nucleus, a small fraction was also detectable in the cytosolic fraction. The amount in the cytosol may still be an overestimation, as some of these mRNAs can originate from nuclei that ruptured during the fractionation experiment. Indeed, very little *SR30.2* was detected on purified ribosomes, in agreement with a previous study that systematically examined the association of *SR* splicing variants with ribosomes (Palusa and Reddy, 2015). The weak ribosomal association explains why no corresponding protein variant was detectable upon constitutive expression of this cDNA in stably transformed Arabidopsis. Even enforced expression in transient assays yielded no or very low amount of SR30.2 protein, while SR30.1 always accumulated to high levels. Taken together, these data suggest that either *SR30.2* is almost fully retained in the nucleus, or, in case some export to the cytosol occurs, an additional mechanism may actively restrain this transcript variant from translation. The full absence of translation of this splicing variant is also supported by its NMD immunity, despite the presence of strong NMD-eliciting features. NMD immunity of *SR30.2* has been demonstrated by analyzing the levels of the individual *SR30* variants in two NMD-impaired mutants, *lba1* (Yoine et al., 2006) and *upf3* (Hori and Watanabe, 2005), in this study and a previous transcriptome-wide comparison of AS patterns between controls and four different types of NMD impairment (Drechsel et al., 2013). In contrast, another study suggested that *SR30.2* is an NMD target, based on an increased ratio of *SR30.2*/*SR30.1* in a *upf3* mutant compared to the wild type (Palusa and Reddy, 2010). However, as this previous study only considered the AS ratio change in a single mutant, and since many signals can alter AS of the *SR30* pre-mRNA (also see below), a change on the level of AS rather than transcript turnover seems to be a more likely explanation for the observation by Palusa and Reddy (2010). In summary, our data strongly suggest that the AS switch in *SR30* functions in quantitative control of gene expression. Remarkably, the protein-coding variant *SR30.1* is subject to rapid decay. This high turnover rate enables a fast change in transcript steady state levels upon shifting the AS of the *SR30* pre-mRNA, quickly adjusting expression of this splicing regulator.

Fine-Tuning *SR30* Expression via AS in Development and Stress Response

AS of the *SR30* pre-mRNA is tightly regulated during development and in response to stresses. We have shown in a previous study (Hartmann et al., 2016) and this report that AS of *SR30* is regulated in response to light and sugar availability. In darkness, mainly *SR30.2* is generated, whereas light and sugar trigger predominant splicing to the protein-coding variant *SR30.1*. Profiling the response over a period of 24 h suggested that this AS switch reaches its maximum at ~6 h and then is partially reverted, possibly as part of a feedback loop. Changes in *SR30* AS have also been observed during development of light-grown seedlings and in comparison of different plant tissues (Lopato et al., 1999; Palusa et al., 2007). Furthermore, several studies demonstrate that the AS output of *SR30* is highly responsive to stress, with heat (Palusa et al., 2007; Filichkin et al., 2010), high light (Tanabe et al., 2007; Filichkin et al., 2010), and NaCl (Tanabe et al., 2007; Filichkin et al., 2010) all resulting in a shift toward *SR30.1*.

Generation of an antibody raised against the endogenous SR30 protein allowed us to demonstrate that the light-induced shift in splicing to *SR30.1* correlates with increased SR30 protein levels, being most pronounced in the comparison of dark- and light-grown plants. Both endogenous SR30 and several transgene-derived tagged versions of it were detected at an apparent M_r that is ~10 kDa above the theoretical size. A similar shift in the size of the SR30 protein upon immunodetection was previously reported and phosphatase treatment has been described to cause faster migration of the protein (Lopato et al., 1999). An elevated apparent M_r has also been observed for other related factors (Golovkin and Reddy, 1998; Ali et al., 2003).

Our subcellular localization studies using fluorescent protein fusions of SR30.1 confirmed its previously reported presence in the nucleoplasm and nuclear speckles (Fang et al., 2004; Lorković et al., 2004), a pattern also observed for several other SR proteins (Fang et al., 2004; Lorković et al., 2004; Tillemans et al., 2005) and SR45 (Ali et al., 2003). In another study, subcellular distribution of At-SR30.1 fused to red fluorescent protein has been examined in onion epidermal cells (Mori et al., 2012). In contrast to our findings in Arabidopsis, a substantial proportion of the fusion protein was present in the cytosol of onion epidermal cells, possibly due to the heterologous expression. Interestingly, chemical inhibition of phosphorylation suppressed nuclear localization of the SR30 protein fusion, which accumulated under these conditions in large structures within the cytosol (Mori et al., 2012). Further work will be needed to determine if interference with phosphorylation similarly affects SR30 localization in Arabidopsis. Furthermore, we observed that the extent of speckle localization varied between cells, which is in line with the highly dynamic nature of nuclear speckles formed by several SR- and SR-like proteins (Ali et al., 2003; Fang et al., 2004; Tillemans et al., 2005, 2006). Enforcing expression of SR30.2 revealed an identical localization of the fluorescent protein fusion in the nuclear compartments as observed for SR30.1.

Constitutive overexpression of a genomic construct of *SR30* has been previously shown to result mainly in splicing to the *SR30.2* variant (Lopato et al., 1999), possibly as part of a feedback control on the AS level, as it has been demonstrated for other splicing regulators, e.g. GRPs (Staiger et al., 2003; Schöning et al., 2008) and PTBs (Stauffer et al., 2010; Wachter et al., 2012). Coexpressing a genomic *SR30* construct with the cds of the major *SR30* splicing variants allowed us to corroborate the assumption of an AS shift toward *SR30.2* under conditions of elevated SR30 protein levels. Remarkably, constitutive coexpression of SR30.1 or SR30.2 with the splicing reporter similarly shifted its AS to the unproductive variant. Based on the comparable splicing regulatory effect and subcellular localization of the artificially expressed SR30.1 and SR30.2, distinct functions of these variants seem unlikely, even if the SR30.2 protein were generated in planta under any condition. In contrast, splicing variant-specific complementation of defects in petal development and root growth has been found for the *sr45-1* mutant (Zhang and Mount, 2009).

Feedback control of SR30 expression on the level of AS can also explain the transient AS response to light and other changes in growth conditions. Accordingly, a shift in AS to *SR30.1* is expected to result in elevated levels and activity of SR30 protein, which in turn should alter splicing of the *SR30* pre-mRNA toward the unproductive *SR30.2* variant. Furthermore, evidence for SR30-mediated AS regulation of its homolog SR34 and other genes has been previously provided, based on changes in their splicing patterns in the *SR30* overexpression lines (Lopato et al., 1999). A recent study aiming at elucidating the physiological functions of SR proteins generated multiple mutants for all subfamilies of SR proteins (Yan et al., 2017). While a quintuple mutant in SC35 and SCL genes displays pleiotropic alterations in plant morphology and development, no phenotypic changes were observed for the other mutants, including the *sr* quadruple mutant that is supposedly defective in the expression of the related factors *SR34*, *SR34a*, *SR34b*, and *SR30*. However, our analysis of the T-DNA insertion line SALK_116747C in *SR30*, which was used by Yan et al. (2017), revealed no difference in the *SR30* expression pattern compared to the wild type (Supplemental Fig. S3A), suggesting that the *sr* quadruple mutant generated by Yan et al. (2017) is, at least for *SR30*, not a knockout. Besides analyzing full knockout mutants, it will be of interest to examine phenotypes of *sr* mutants under specific growth conditions including stress regimes. In line with a critical function of *SR30*, its overexpression resulted in several morphological and developmental defects, including late flowering, reduced apical dominance, and changes in rosette leaf size (Lopato et al., 1999). This finding underscores the importance of tight regulation of *SR30* expression, which we have demonstrated in this work to be based on the intricate interplay of nuclear and cytosolic events in RNA metabolism.

MATERIALS AND METHODS

Plant Cultivation and Experiments

Arabidopsis (*Arabidopsis thaliana*) Col-0 seeds sterilized in 3.75% NaOCl and 0.01% Triton X-100 were grown on or in 0.5× Murashige and Skoog (MS) medium with supplements added as described below. Solid medium contained 0.8% phytoagar (Duchefa). Upon stratification for at least 2 d at 4°C, germination was induced in white light for 2 h. All darkness samples were taken in green light. For light experiments (Fig. 1), seeds were plated on solid medium containing 2% Suc. Six-day-old, dark-grown seedlings were exposed to white, blue, or red light, or kept in darkness for the indicated period. For transfer experiments (Fig. 6B), seedlings were grown on solid medium without Suc and kept in darkness for 6 d after induction of germination. Under green light, seedlings were transferred to liquid 0.5× MS medium with or without supplements as indicated and incubated in darkness or light for the time stated. For the RNA half-life assay (Fig. 2B), seedlings were cultivated in 100 mL liquid medium under long-day conditions on a shaker at 115 rpm for 7 d. The seedlings were rinsed with water, transferred into 150 μg/mL cordycepin (Sigma-Aldrich) solution, and then sampled after 1, 2, 3, and 4 h. For the other experiments, seedlings were cultivated for the indicated time under long-day conditions on solid medium containing 2% Suc.

Light Conditions

Continuous white light was used at an intensity of ~130 μmol m^{-2} s^{-1}. Monochromatic light from LED fields (Flora LED; CLF Plant Climatics) had the following specifications: blue 420 to 550 nm, maximum at 463 nm, full width at half maximum 22.2 nm, intensity ~6 μmol m^{-2} s^{-1}; red 620 to 730 nm, maximum at 671 nm, full width at half maximum 25 nm, intensity ~18 μmol m^{-2} s^{-1}. Intensities were measured with a Skye SKR1850 (Skye Instruments) and are limited to photosynthetically active radiation.

Subcellular Fractionation

Subcellular fractionation was performed according to a protocol provided by M. Amorim and S. Laubinger (de Francisco Amorim et al., 2017). Briefly, 2 g of plant material was ground under liquid nitrogen cooling and suspended in 4 mL HONDA buffer (20 mM HEPES, KOH, pH 7.4, 0.44 M Suc, 1.25% Ficoll 400, 2.5% Dextran T40, 10 mM $MgCl_2$, 0.5% Triton X-100, 1 mM PMSF, 5 mM DTT, 50 units/mL RiboLock [Thermo Fisher Scientific], and 1× Complete protease inhibitor [Roche]). All following steps were performed at 4°C. The sample plus 1 mL HONDA buffer used for rinsing was filtered through Miracloth (Calbiochem; 22–25 μm), resulting in the total fraction. The sample was centrifuged at 1,500*g* for 10 min to separate the nuclei and the cytosolic fraction. The supernatant was transferred into a fresh tube and centrifuged at 13,000*g* for 15 min. The resulting supernatant corresponded to the cytosolic fraction. The pellet from the 1,500*g* centrifugation was resuspended in 1 mL HONDA buffer using a Pasteur pipette and centrifuged at 1,800*g* for 5 min. This washing step was repeated four to five times until the supernatant became clear. Finally, the pellet was suspended in 400 μL HONDA buffer (nuclei fraction). Three hundred and one hundred microliters were used for RNA and protein extraction, respectively. Samples taken for RNA isolation were thoroughly mixed with 2 volumes of 8 M guanidinium hydrochloride and 3 volumes of 100% ethanol. The RNA was precipitated over night at −20°C and pelleted at 16,000*g* for

50 min. The supernatant was removed, the pellet was dried at room temperature for 20 min and used for RNA isolation using a column-based system as described below. Protein samples were mixed with 5× SDS sample buffer (0.3 M Tris-HCl, pH 6.8, 50% glycerol, 5% SDS, 0.05% bromophenol blue, and 100 mM DTT) and denatured at 95°C for 5 min.

Ribosome Immunoprecipitation

Ribosome immunoprecipitation was conducted based on a protocol from Mustroph et al. (2013). Briefly, 2 g of seedlings was ground under liquid nitrogen cooling and mixed with 5 mL polysome extraction buffer (200 mM Tris-HCl, pH 9.0, 200 mM KCl, 25 mM EGTA, 36 mM $MgCl_2$, 5 mM DTT, 50 μg/mL cycloheximide, 50 μg/mL chloramphenicol, 0.5 mg/mL heparin, 1% Triton X-100, 1% Tween 20, 1% Brij-35, 1% IGEPAL CA-630, 2% polyethylene glycol 400, 1% deoxycholic acid, 1 mM PMSF, and 50 units/mL RiboLock). All subsequent steps were performed at 4°C. The sample was centrifuged at 16,000*g* for 15 min, followed by filtration of the supernatant through Miracloth (Calbiochem; 22–25 μm) and another centrifugation step at 16,000*g* for 15 min. The input sample was taken from the supernatant. One hundred and fifty microliters of Protein G coupled Dynabeads (Life Technologies) was washed twice with 1.5 mL washing buffer (WB; 200 mM Tris-HCl, pH 9.0, 200 mM KCl, 25 mM EGTA, 36 mM $MgCl_2$, 5 mM DTT, 50 μg/mL cycloheximide, 50 μg/mL chloramphenicol, and 50 units/mL RiboLock), resuspended in 150 μL WB, and incubated with 5 μL α-FLAG antibody solution (Sigma-Aldrich) under agitation for 10 min at room temperature. The beads were washed once more with WB and resuspended in 150 μL WB. The suspension of α-FLAG-coated Dynabeads was added to the remaining supernatant of the seedling samples and incubated for 2 h while shaking gently. The beads were separated from the supernatant using a magnet and washed with 5 mL polysome extraction buffer followed by three washes with WB. Finally, the tagged ribosomes were eluted with 400 μL WB containing 200 ng/μL FLAG peptide (Sigma-Aldrich) for 30 min while shaking. The elution fraction was split into 300 and 100 μL for RNA and protein isolation, respectively. The RNA and protein samples were further processed as described for the subcellular fractionation.

RNA Isolation, Reverse Transcription, and PCR

RNA was isolated with the Universal RNA Purification Kit (EURx) in combination with an on-column DNase digest according to the manufacturer's instructions and eluted in 40 μL RNase-free water. RevertAid Premium (Thermo Fisher Scientific) or AMV Reverse Transcriptase Native (EURx) was used for reverse transcription, mostly following the manufacturers' specifications but using the maximum volume of RNA possible in the reaction. Unless stated otherwise, dT_{20} primer was used.

Coamplification PCRs were performed using a homemade Taq polymerase and following standard protocols. Resulting RT-PCR products were separated on agarose gels and stained with ethidium bromide solution. Gel pictures were taken under UV light and, if needed, modified using Adobe Photoshop auto-contrast function. Quantification of coamplified PCR products was performed using the Agilent DNA1000 kit and 2100 Bioanalyzer. The CFX384 real-time PCR system (Bio-Rad) and MESA BLUE qPCR MasterMix Plus (Eurogentec) were used for relative quantification of individual cDNAs. *PROTEIN PHOSPHATASE 2A* (*PP2A*, *AT1G13320*) was used as a reference transcript, except for the half-life assay, for which *ACTIN7* (*At5G09810*) was used as reference. A detailed quantitative PCR protocol is described by Stauffer et al. (2010).

Cloning Procedures

SR30 overexpression constructs for immunoblots were based on the vector pBinAR (Höfgen and Willmitzer, 1992). All primers used for cloning are listed in Supplemental Table S2. For cds constructs, inserts were amplified from cDNA using LH163/211 (SR30.1) or LH163/212 (SR30.2) omitting the STOP codon and cloned into a pBinAR containing HA3-STOP via *Bam*HI/*Xba*I. The inserts of the cDNA constructs were amplified each in two parts inserting an HA-tag at the C-terminus and removing the STOP codon with LH186/187 and LH188/189 (SR30.1) or LH186/190 and LH191/189 (SR30.2). The respective parts were combined using the corresponding outer primers. Cloning into *Bam*HI/*Sal*I digested pBinAR was done via *Bam*HI/*Xho*I. To generate HA3-tagged versions, the inserts both were amplified in two parts and HA3 added using LH186/312 and LH311/189. Insertion into pBinAR was done as described above for the untagged cDNA constructs. For constructs used for confocal microscopy, splice variants of *SR30* were amplified with primers LH159/160 or LH159/161, respectively, omitting the STOP codon, and recombined into pDONR201, then pB7CWG2 or pB7YWG2 (Karimi et al., 2002) using the Gateway system (Invitrogen). The genomic reporter used in the splice assay (Fig. 5) was amplified using primers LH163/169 inserting the C-terminal HA-tag and cloned into *Bam*HI/*Sal*I digested pBinAR via *Bam*HI/*Xho*I. The splice form-specific Flag-tagged cds constructs were cloned similarly using primers LH163/164 and LH163/165, respectively. The amiRNA was designed using the web tool WMD3 (http://wmd3.weigelworld.org; Ossowski et al., 2008) and cloned following the available protocol (http://wmd3.weigelworld.org/downloads/Cloning_of_artificial_microRNAs.pdf) using primers LH192-195. After extension of the partial attachment sites with primers ES32/33, the precursor was recombined into pDONR201, then pB7WG2 (Karimi et al., 2002) using the Gateway system (Invitrogen). For expression of recombinant SR30 for immunization, *SR30.2* cds was amplified using LH163/182 and cloned into pQE30 (Qiagen) via *Bam*HI/*Xho*I. Sequencing *SR30*, we discovered an insertion relative to the TAIR10 reference sequence. One G nucleotide was inserted between positions 2926 and 2927 of the annotated gene in the 11th intron. We found this insertion both in our wild-type line and the *lba1* mutant.

Plant Transformation

Heterotrophic cell culture protoplasts were transformed according to a previously published protocol (Schütze et al., 2009) with 2 μg of each plasmid and kept in darkness for 2 d before microscopy. *Nicotiana benthamiana* leaves were transiently transformed by leaf infiltration as previously described (Wachter et al., 2007) using transformed agrobacteria of an optical density 0.8 at 600 nm in water. Cotransformation of luciferase or one of the splicing variants with the reporter was achieved by mixing the respective bacterial suspensions 1:1 before infiltration. Cotransformation of the reporter with the luciferase control or with one of the splicing variants was always done on corresponding leaf halves for normalization purposes. Infiltrated plants were grown for additional 2 d before sampling. Arabidopsis plants were stably transformed by the floral dip method (Clough and Bent, 1998).

Antibody Generation

Escherichia coli M15 expressing *SR30.2* in the vector pQE30 were grown in 3 L Terrific Broth medium to an optical density >1 at 37°C. Protein expression was induced with 1 mM isopropyl β-D-thiogalactopyranoside and the culture further incubated at 37°C overnight. All following steps were done at 4°C or on ice unless specified otherwise. The cells were spun down and resuspended in cold lysis-equilibration-wash buffer (LEW; 300 mM NaCl and 50 mM NaH_2PO_4, pH 8.0), then lysed using a cooled French pressure cell (Aminco; 3× 1,000 psi). The lysate was treated with 50 μg/mL DNase for 20 min at room temperature under agitation and then centrifuged (10,000*g*, 30 min). The pellet was washed once with cold LEW, then resuspended in 25 mL denaturing solubilization buffer (DSB; 300 mM NaCl, 50 mM NaH_2PO_4, pH 8.0, and 8 M urea), incubated on a wheel shaker for 1 h, and spun at room temperature for 40 min at 10,000*g* or until supernatant was clear. The supernatant was added to Protino Ni-TED resin (Macherey-Nagel) prepared according to the manufacturer's instructions and incubated on a wheel shaker for 1 h at room temperature. The column was drained by gravity at room temperature and the flow-through was collected. At room temperature, the resin was washed with 200 mL DSB, and protein was eluted three times with 3 mL 150 mM and three times with 3 mL 200 mM imidazole-containing DSB. Elution fractions were combined, diluted with 5 mL LEW per mL elution fraction, and incubated on a wheel shaker overnight. Precipitated protein was spun down, resuspended in 2× SDS sample buffer, and denatured at 95°C for 10 min. Protein concentration was estimated by comparing band intensities on a gel to marker bands. Approximately 200 μg protein per lane was loaded on a 12% polyacrylamide gel. After Coomassie staining, the prominent band was excised excluding a slightly smaller band, and the gel pieces were washed in water until the pH was neutral. Rabbits were immunized six times with the gel-bound protein (BioGenes). The antibody was affinity purified from raw sera using membrane-bound antigen as described before (Rühl et al., 2012), but partly using a 1:1 dilution of 7 mL serum in one purification.

Protein Extraction, Immunoprecipitation, and Immunoblot Analyses

Starting material from infiltrated *N. benthamiana* leaves was ~100 mg, and 200 to 300 mg Arabidopsis seedlings was used per extraction. For immunoblot analyses, proteins were extracted as described previously (Rühl et al., 2012), using an extraction buffer containing 65 mM KCl, 15 mM NaCl, 10 mM HEPES (pH 7.6), 10 mM Na_2EDTA, 5 mM DTT, 4 mM ATP, 1× phosphatase inhibitor mix (Serva), and 1× Complete (Roche; after Zahler et al., 1992). All extracts were cleared by centrifugation at 4°C for ~20 min at ~15,000*g*.

Using Protein G-coupled Dynabeads (Life Technologies), α-SR30 was coupled to the beads in PBS-T by incubation under agitation for 10 min at room temperature. The beads were washed once with PBS-T. Protein extract was added to the beads and protein was allowed to bind to the beads for 1 h at room temperature on a wheel shaker. The beads were washed three times using the extraction buffer and transferred to a fresh tube in a fourth washing step. Protein bound to Dynabeads was eluted at 95°C in 5× SDS sample buffer for 10 min while mixing.

SDS-PAGE and semidry immunoblotting were performed according to standard protocols. For detection, the following commercial antibodies were used: rabbit α-histone H3 (Agrisera), rabbit α-UGPase (Agrisera), rabbit α-FLAG (Sigma-Aldrich), mouse α-HA (Sigma-Aldrich), α-mouse-peroxidase (Sigma-Aldrich), and α-rabbit-peroxidase (Sigma-Aldrich). Chemiluminescence detection used Super or Ultra Signal West Dura (Pierce).

Confocal Microscopy

Microscopy was conducted with a TCS SP2 AOBS (Leica). The excitation (ex.) and emission (em.) settings were as follows: YFP 514 nm (ex.), 524 to 575 nm (em.) and DsRED 561 nm (ex.), 575 to 641 nm (em.) in Figure 4A; CFP 405 nm (ex.), 453 to 511 nm (em.) and YFP 514 nm (ex), 566 to 617 nm (em.) in Figure 4B; CFP 405 nm (ex.), 457 to 540 nm (em.) and YFP as for Figure 4A in Figure 4, C and D. The protoplasts were scanned in sequential mode, with the exception of the one shown in Figure 4B.

Accession Numbers

The following mutants have been used in different experiments: *sr30* (GK325-E11, N322146), *lba1* (Yoine et al., 2006), *upf3-1* (Hori and Watanabe, 2005), 35S: HF-RPL18 (N66056; Zanetti et al., 2005), *sop2-1* (Hématy et al., 2016), *mtr3* (also referred to as *rrp41l*; Yang et al., 2013), *hen2-4* and *mtr4-1* (Lange et al., 2011), *ski2-6* (Zhao and Kunst, 2016), *xrn4-5* (Souret et al., 2004), and *xrn2-1 xrn4-6*, *xrn3-3 xrn4-6*, and *fry1-6* (Gy et al., 2007). The following genes have been analyzed: *AT1G09140* (*SR30*), *AT2G37340* (*RS2Z33*), *AT5G37055* (*SEF*), *AT1G13320* (*PP2A*), and *At5G09810* (*ACTIN7*).

Supplemental Data

The following supplemental materials are available.

Supplemental Figure S1. Sequences of *SR30* Splicing Variants Analyzed in this Work.

Supplemental Figure S2. Levels of *SR30* Splicing Variants in RNA Degradation Mutants.

Supplemental Figure S3. SR30 Expression in T-DNA Mutants and in Response to Light.

Supplemental Figure S4. Detection of SR30 Fused to Fluorescent Proteins.

Supplemental Figure S5. Sequences of Splicing Variants from Light-Regulated AS Events in *SR30*.

Supplemental Figure S6. *SR30* Splicing Variant Patterns in Response to Light, Sugar, and *SR30* Overexpression.

Supplemental Figure S7. Examples of *SR* Genes with Long Introns Containing NMD-Triggering Cassette Exons.

Supplemental Table S1. *SR30* Transcript Levels and Segregation of Lines upon Splicing Variant-Specific Misexpression of *SR30*.

Supplemental Table S2. Sequences of DNA Oligos Used in This Study.

ACKNOWLEDGMENTS

We thank the Nottingham Arabidopsis Stock Centre for providing seeds of the *sr30*, *lba1*, and *upf3-1* mutants and of the 35S:HF-RPL18 line. Seeds of the *xrn* mutants were kindly provided by Hervé Vaucheret. We acknowledge Dominique Gagliardi and Heike Lange for providing seeds of the other RNA decay mutants and for discussion of the corresponding data. Furthermore, we thank Hsin-Chieh Lee for providing samples for the RNA stability assay, and Marcella Amorim and Sascha Laubinger for sharing an unpublished protocol for the subcellular fractionation experiment. We also thank Eva Stauffer and Gabriele Drechsel for help with the confocal microscope, and Gabriele Wagner and Natalie Faiss for laboratory assistance. We thank Xaq Pitkow for input on the graphical design of Figure 7. Technical support by the central facilities of the Center for Plant Molecular Biology (University of Tübingen) is acknowledged.

Received September 5, 2017; accepted February 16, 2018; published March 1, 2018.

LITERATURE CITED

Ali GS, Golovkin M, Reddy AS (2003) Nuclear localization and in vivo dynamics of a plant-specific serine/arginine-rich protein. Plant J **36:** 883–893

Ali GS, Palusa SG, Golovkin M, Prasad J, Manley JL, Reddy AS (2007) Regulation of plant developmental processes by a novel splicing factor. PLoS One **2:** e471

Bardou F, Ariel F, Simpson CG, Romero-Barrios N, Laporte P, Balzergue S, Brown JW, Crespi M (2014) Long noncoding RNA modulates alternative splicing regulators in Arabidopsis. Dev Cell **30:** 166–176

Boothby TC, Zipper RS, van der Weele CM, Wolniak SM (2013) Removal of retained introns regulates translation in the rapidly developing gametophyte of Marsilea vestita. Dev Cell **24:** 517–529

Braunschweig U, Gueroussov S, Plocik AM, Graveley BR, Blencowe BJ (2013) Dynamic integration of splicing within gene regulatory pathways. Cell **152:** 1252–1269

Carvalho RF, Szakonyi D, Simpson CG, Barbosa IC, Brown JW, Baena-González E, Duque P (2016) The Arabidopsis SR45 splicing factor, a negative regulator of sugar signaling, modulates SNF1-Related Protein Kinase 1 stability. Plant Cell **28:** 1910–1925

Chen M, Manley JL (2009) Mechanisms of alternative splicing regulation: insights from molecular and genomics approaches. Nat Rev Mol Cell Biol **10:** 741–754

Chin A, Lécuyer E (2017) RNA localization: Making its way to the center stage. Biochim Biophys Acta **1861:** 2956–2970

Clough SJ, Bent AF (1998) Floral dip: a simplified method for Agrobacterium-mediated transformation of Arabidopsis thaliana. Plant J **16:** 735–743

Cook-Andersen H, Wilkinson MF (2015) Molecular biology: Splicing does the two-step. Nature **521:** 300–301

Day IS, Golovkin M, Palusa SG, Link A, Ali GS, Thomas J, Richardson DN, Reddy AS (2012) Interactions of SR45, an SR-like protein, with spliceosomal proteins and an intronic sequence: insights into regulated splicing. Plant J **71:** 936–947

de Francisco Amorim M, Willing E-M, Droste-Borel I, Macek B, Schneeberger K, Laubinger S (2017) Arabidopsis U1 snRNP subunit LUC7 functions in alternative splicing and preferential removal of terminal introns. bioRxiv doi.org/10.1101/150805

Dolata J, Guo Y, Kołowerzo A, Smoliński D, Brzyżek G, Jarmołowski A, Świeżewski S (2015) NTR1 is required for transcription elongation checkpoints at alternative exons in Arabidopsis. EMBO J **34:** 544–558

Dominguez D, Tsai YH, Weatheritt R, Wang Y, Blencowe BJ, Wang Z (2016) An extensive program of periodic alternative splicing linked to cell cycle progression. eLife **5:** e10288

Drechsel G, Kahles A, Kesarwani AK, Stauffer E, Behr J, Drewe P, Rätsch G, Wachter A (2013) Nonsense-mediated decay of alternative precursor mRNA splicing variants is a major determinant of the Arabidopsis steady state transcriptome. Plant Cell **25:** 3726–3742

Duff MO, Olson S, Wei X, Garrett SC, Osman A, Bolisetty M, Plocik A, Celniker SE, Graveley BR (2015) Genome-wide identification of zero nucleotide recursive splicing in Drosophila. Nature **521:** 376–379

Fang Y, Hearn S, Spector DL (2004) Tissue-specific expression and dynamic organization of SR splicing factors in Arabidopsis. Mol Biol Cell **15:** 2664–2673

Filichkin SA, Priest HD, Givan SA, Shen R, Bryant DW, Fox SE, Wong WK, Mockler TC (2010) Genome-wide mapping of alternative splicing in *Arabidopsis thaliana*. Genome Res **20:** 45–58

Filichkin SA, Cumbie JS, Dharmawardhana P, Jaiswal P, Chang JH, Palusa SG, Reddy AS, Megraw M, Mockler TC (2015) Environmental stresses modulate abundance and timing of alternatively spliced circadian transcripts in Arabidopsis. Mol Plant **8:** 207–227

Ghosh S, Marchand V, Gáspár I, Ephrussi A (2012) Control of RNP motility and localization by a splicing-dependent structure in oskar mRNA. Nat Struct Mol Biol **19:** 441–449

Göhring J, Jacak J, Barta A (2014) Imaging of endogenous messenger RNA splice variants in living cells reveals nuclear retention of transcripts inaccessible to nonsense-mediated decay in Arabidopsis. Plant Cell **26:** 754–764

Golovkin M, Reddy AS (1998) The plant U1 small nuclear ribonucleoprotein particle 70K protein interacts with two novel serine/arginine-rich proteins. Plant Cell **10:** 1637–1648

Gueroussov S, Gonatopoulos-Pournatzis T, Irimia M, Raj B, Lin ZY, Gingras AC, Blencowe BJ (2015) An alternative splicing event amplifies evolutionary differences between vertebrates. Science **349:** 868–873

Gy I, Gasciolli V, Lauressergues D, Morel JB, Gombert J, Proux F, Proux C, Vaucheret H, Mallory AC (2007) Arabidopsis FIERY1, XRN2, and XRN3 are endogenous RNA silencing suppressors. Plant Cell **19:** 3451–3461

Hachet O, Ephrussi A (2004) Splicing of oskar RNA in the nucleus is coupled to its cytoplasmic localization. Nature **428:** 959–963

Hartmann L, Drewe-Boß P, Wießner T, Wagner G, Geue S, Lee HC, Obermüller DM, Kahles A, Behr J, Sinz FH, Rätsch G, Wachter A (2016) Alternative splicing substantially diversifies the transcriptome during early photomorphogenesis and correlates with the energy availability in Arabidopsis. Plant Cell **28:** 2715–2734

Hatton AR, Subramaniam V, Lopez AJ (1998) Generation of alternative Ultrabithorax isoforms and stepwise removal of a large intron by resplicing at exon-exon junctions. Mol Cell **2:** 787–796

Hématy K, Bellec Y, Podicheti R, Bouteiller N, Anne P, Morineau C, Haslam RP, Beaudoin F, Napier JA, Mockaitis K, et al (2016) The zinc-finger protein SOP1 is required for a subset of the nuclear exosome functions in Arabidopsis. PLoS Genet **12:** e1005817

Höfgen R, Willmitzer L (1992) Transgenic potato plants depleted for the major tuber protein patatin via expression of antisense RNA. Plant Sci **87:** 45–54

Hori K, Watanabe Y (2005) UPF3 suppresses aberrant spliced mRNA in Arabidopsis. Plant J **43:** 530–540

James AB, Syed NH, Bordage S, Marshall J, Nimmo GA, Jenkins GI, Herzyk P, Brown JW, Nimmo HG (2012) Alternative splicing mediates responses of the Arabidopsis circadian clock to temperature changes. Plant Cell **24:** 961–981

Kalyna M, Lopato S, Barta A (2003) Ectopic expression of atRSZ33 reveals its function in splicing and causes pleiotropic changes in development. Mol Biol Cell **14:** 3565–3577

Kalyna M, Lopato S, Voronin V, Barta A (2006) Evolutionary conservation and regulation of particular alternative splicing events in plant SR proteins. Nucleic Acids Res **34:** 4395–4405

Kalyna M, Simpson CG, Syed NH, Lewandowska D, Marquez Y, Kusenda B, Marshall J, Fuller J, Cardle L, McNicol J, et al (2012) Alternative splicing and nonsense-mediated decay modulate expression of important regulatory genes in Arabidopsis. Nucleic Acids Res **40:** 2454–2469

Karimi M, Inze D, Depicker A (2002) GATEWAY vectors for Agrobacterium-mediated plant transformation. Trends Plant Sci **7:** 193–195

Kerényi Z, Mérai Z, Hiripi L, Benkovics A, Gyula P, Lacomme C, Barta E, Nagy F, Silhavy D (2008) Inter-kingdom conservation of mechanism of nonsense-mediated mRNA decay. EMBO J **27:** 1585–1595

Kim SH, Koroleva OA, Lewandowska D, Pendle AF, Clark GP, Simpson CG, Shaw PJ, Brown JW (2009) Aberrant mRNA transcripts and the nonsense-mediated decay proteins UPF2 and UPF3 are enriched in the Arabidopsis nucleolus. Plant Cell **21:** 2045–2057

Kriechbaumer V, Wang P, Hawes C, Abell BM (2012) Alternative splicing of the auxin biosynthesis gene YUCCA4 determines its subcellular compartmentation. Plant J **70:** 292–302

Lamesch P, Berardini TZ, Li D, Swarbreck D, Wilks C, Sasidharan R, Muller R, Dreher K, Alexander DL, Garcia-Hernandez M, et al (2012) The Arabidopsis Information Resource (TAIR): improved gene annotation and new tools. Nucleic Acids Res **40:** D1202–D1210

Lange H, Sement FM, Gagliardi D (2011) MTR4, a putative RNA helicase and exosome co-factor, is required for proper rRNA biogenesis and development in *Arabidopsis thaliana*. Plant J **68:** 51–63

Li Q, Zheng S, Han A, Lin CH, Stoilov P, Fu XD, Black DL (2014) The splicing regulator PTBP2 controls a program of embryonic splicing required for neuronal maturation. eLife **3:** e01201

Li S, Yamada M, Han X, Ohler U, Benfey PN (2016) High-resolution expression map of the Arabidopsis root reveals alternative splicing and lincRNA regulation. Dev Cell **39:** 508–522

Liu N, Dai Q, Zheng G, He C, Parisien M, Pan T (2015) N(6)-methyladenosine-dependent RNA structural switches regulate RNA-protein interactions. Nature **518:** 560–564

Lopato S, Kalyna M, Dorner S, Kobayashi R, Krainer AR, Barta A (1999) atSRp30, one of two SF2/ASF-like proteins from *Arabidopsis thaliana*, regulates splicing of specific plant genes. Genes Dev **13:** 987–1001

Lorković ZJ, Hilscher J, Barta A (2004) Use of fluorescent protein tags to study nuclear organization of the spliceosomal machinery in transiently transformed living plant cells. Mol Biol Cell **15:** 3233–3243

Mandadi KK, Scholthof KB (2015) Genome-wide analysis of alternative splicing landscapes modulated during plant-virus interactions in *Brachypodium distachyon*. Plant Cell **27:** 71–85

Marquez Y, Brown JW, Simpson C, Barta A, Kalyna M (2012) Transcriptome survey reveals increased complexity of the alternative splicing landscape in Arabidopsis. Genome Res **22:** 1184–1195

Meyer K, Köster T, Nolte C, Weinholdt C, Lewinski M, Grosse I, Staiger D (2017) Adaptation of iCLIP to plants determines the binding landscape of the clock-regulated RNA-binding protein AtGRP7. Genome Biol **18:** 204

Mohr SE, Dillon ST, Boswell RE (2001) The RNA-binding protein Tsunagi interacts with Mago Nashi to establish polarity and localize oskar mRNA during Drosophila oogenesis. Genes Dev **15:** 2886–2899

Mori T, Yoshimura K, Nosaka R, Sakuyama H, Koike Y, Tanabe N, Maruta T, Tamoi M, Shigeoka S (2012) Subcellular and subnuclear distribution of high-light responsive serine/arginine-rich proteins, atSR45a and atSR30, in *Arabidopsis thaliana*. Biosci Biotechnol Biochem **76:** 2075–2081

Mustroph A, Zanetti ME, Girke T, Bailey-Serres J (2013) Isolation and analysis of mRNAs from specific cell types of plants by ribosome immunopurification. Methods Mol Biol **959:** 277–302

Newmark PA, Boswell RE (1994) The mago nashi locus encodes an essential product required for germ plasm assembly in Drosophila. Development **120:** 1303–1313

Ossowski S, Schwab R, Weigel D (2008) Gene silencing in plants using artificial microRNAs and other small RNAs. Plant J **53:** 674–690

Palacios IM, Gatfield D, St Johnston D, Izaurralde E (2004) An eIF4AIII-containing complex required for mRNA localization and nonsense-mediated mRNA decay. Nature **427:** 753–757

Palusa SG, Ali GS, Reddy AS (2007) Alternative splicing of pre-mRNAs of Arabidopsis serine/arginine-rich proteins: regulation by hormones and stresses. Plant J **49:** 1091–1107

Palusa SG, Reddy AS (2010) Extensive coupling of alternative splicing of pre-mRNAs of serine/arginine (SR) genes with nonsense-mediated decay. New Phytol **185:** 83–89

Palusa SG, Reddy AS (2015) Differential recruitment of splice variants from SR pre-mRNAs to polysomes during development and in response to stresses. Plant Cell Physiol **56:** 421–427

Pan Q, Shai O, Lee LJ, Frey BJ, Blencowe BJ (2008) Deep surveying of alternative splicing complexity in the human transcriptome by high-throughput sequencing. Nat Genet **40:** 1413–1415

Penfield S, Josse EM, Halliday KJ (2010) A role for an alternative splice variant of PIF6 in the control of Arabidopsis primary seed dormancy. Plant Mol Biol **73:** 89–95

Reddy AS, Marquez Y, Kalyna M, Barta A (2013) Complexity of the alternative splicing landscape in plants. Plant Cell **25:** 3657–3683

Remy E, Cabrito TR, Baster P, Batista RA, Teixeira MC, Friml J, Sá-Correia I, Duque P (2013) A major facilitator superfamily transporter plays a dual role in polar auxin transport and drought stress tolerance in Arabidopsis. Plant Cell **25:** 901–926

Rühl C, Stauffer E, Kahles A, Wagner G, Drechsel G, Rätsch G, Wachter A (2012) Polypyrimidine tract binding protein homologs from Arabidopsis are key regulators of alternative splicing with implications in fundamental developmental processes. Plant Cell **24:** 4360–4375

Sanchez SE, Petrillo E, Beckwith EJ, Zhang X, Rugnone ML, Hernando CE, Cuevas JC, Godoy Herz MA, Depetris-Chauvin A, Simpson CG, et al (2010) A methyl transferase links the circadian clock to the regulation of alternative splicing. Nature **468:** 112–116

Schöning JC, Streitner C, Meyer IM, Gao Y, Staiger D (2008) Reciprocal regulation of glycine-rich RNA-binding proteins via an interlocked feedback loop coupling alternative splicing to nonsense-mediated decay in Arabidopsis. Nucleic Acids Res **36:** 6977–6987

Schütze K, Harter K, Chaban C (2009) Bimolecular fluorescence complementation (BiFC) to study protein-protein interactions in living plant cells. Methods Mol Biol **479:** 189–202

Shikata H, Hanada K, Ushijima T, Nakashima M, Suzuki Y, Matsushita T (2014) Phytochrome controls alternative splicing to mediate light responses in Arabidopsis. Proc Natl Acad Sci USA **111:** 18781–18786

Shikata H, Shibata M, Ushijima T, Nakashima M, Kong S-G, Matsuoka K, Lin C, Matsushita T (2012) The RS domain of Arabidopsis splicing factor RRC1 is required for phytochrome B signal transduction. Plant J **70:** 727–738

Sibley CR, Emmett W, Blazquez L, Faro A, Haberman N, Briese M, Trabzuni D, Ryten M, Weale ME, Hardy J, et al (2015) Recursive splicing in long vertebrate genes. Nature **521:** 371–375

Souret FF, Kastenmayer JP, Green PJ (2004) AtXRN4 degrades mRNA in Arabidopsis and its substrates include selected miRNA targets. Mol Cell **15:** 173–183

Staiger D, Brown JW (2013) Alternative splicing at the intersection of biological timing, development, and stress responses. Plant Cell **25:** 3640–3656

Staiger D, Green R (2011) RNA-based regulation in the plant circadian clock. Trends Plant Sci **16:** 517–523

Staiger D, Zecca L, Wieczorek Kirk DA, Apel K, Eckstein L (2003) The circadian clock regulated RNA-binding protein AtGRP7 autoregulates its expression by influencing alternative splicing of its own pre-mRNA. Plant J **33:** 361–371

Stauffer E, Westermann A, Wagner G, Wachter A (2010) Polypyrimidine tract-binding protein homologues from Arabidopsis underlie regulatory circuits based on alternative splicing and downstream control. Plant J **64:** 243–255

Streitner C, Köster T, Simpson CG, Shaw P, Danisman S, Brown JW, Staiger D (2012) An hnRNP-like RNA-binding protein affects alternative splicing by in vivo interaction with transcripts in Arabidopsis thaliana. Nucleic Acids Res **40:** 11240–11255

Sureshkumar S, Dent C, Seleznev A, Tasset C, Balasubramanian S (2016) Nonsense-mediated mRNA decay modulates FLM-dependent thermosensory flowering response in Arabidopsis. Nat Plants **2:** 16055

Tanabe N, Yoshimura K, Kimura A, Yabuta Y, Shigeoka S (2007) Differential expression of alternatively spliced mRNAs of Arabidopsis SR protein homologs, atSR30 and atSR45a, in response to environmental stress. Plant Cell Physiol **48:** 1036–1049

Thomas J, Palusa SG, Prasad KV, Ali GS, Surabhi GK, Ben-Hur A, Abdel-Ghany SE, Reddy AS (2012) Identification of an intronic splicing regulatory element involved in auto-regulation of alternative splicing of SCL33 pre-mRNA. Plant J **72:** 935–946

Tillemans V, Dispa L, Remacle C, Collinge M, Motte P (2005) Functional distribution and dynamics of Arabidopsis SR splicing factors in living plant cells. Plant J **41:** 567–582

Tillemans V, Leponce I, Rausin G, Dispa L, Motte P (2006) Insights into nuclear organization in plants as revealed by the dynamic distribution of Arabidopsis SR splicing factors. Plant Cell **18:** 3218–3234

Traunmüller L, Gomez AM, Nguyen TM, Scheiffele P (2016) Control of neuronal synapse specification by a highly dedicated alternative splicing program. Science **352:** 982–986

van Eeden FJ, Palacios IM, Petronczki M, Weston MJ, St Johnston D (2001) Barentsz is essential for the posterior localization of oskar mRNA and colocalizes with it to the posterior pole. J Cell Biol **154:** 511–523

Wachter A (2010) Riboswitch-mediated control of gene expression in eukaryotes. RNA Biol **7:** 67–76

Wachter A (2014) Gene regulation by structured mRNA elements. Trends Genet **30:** 172–181

Wachter A, Rühl C, Stauffer E (2012) The role of polypyrimidine tract-binding proteins and other hnRNP proteins in plant splicing regulation. Front Plant Sci **3:** 81

Wachter A, Tunc-Ozdemir M, Grove BC, Green PJ, Shintani DK, Breaker RR (2007) Riboswitch control of gene expression in plants by splicing and alternative 3′ end processing of mRNAs. Plant Cell **19:** 3437–3450

Wang B, Tseng E, Regulski M, Clark TA, Hon T, Jiao Y, Lu Z, Olson A, Stein JC, Ware D (2016) Unveiling the complexity of the maize transcriptome by single-molecule long-read sequencing. Nat Commun **7:** 11708

Wang X, Wu F, Xie Q, Wang H, Wang Y, Yue Y, Gahura O, Ma S, Liu L, Cao Y, et al (2012) SKIP is a component of the spliceosome linking alternative splicing and the circadian clock in Arabidopsis. Plant Cell **24:** 3278–3295

Wu Z, Zhu D, Lin X, Miao J, Gu L, Deng X, Yang Q, Sun K, Zhu D, Cao X, et al (2016) RNA binding proteins RZ-1B and RZ-1C play critical roles in regulating pre-mRNA splicing and gene expression during development in Arabidopsis. Plant Cell **28:** 55–73

Xing D, Wang Y, Hamilton M, Ben-Hur A, Reddy AS (2015) Transcriptome-wide identification of RNA targets of Arabidopsis SERINE/ARGININE-RICH45 uncovers the unexpected roles of this RNA binding protein in RNA processing. Plant Cell **27:** 3294–3308

Yan Q, Xia X, Sun Z, Fang Y (2017) Depletion of Arabidopsis SC35 and SC35-like serine/arginine-rich proteins affects the transcription and splicing of a subset of genes. PLoS Genet **13:** e1006663

Yang M, Zhang B, Jia J, Yan C, Habaike A, Han Y (2013) RRP41L, a putative core subunit of the exosome, plays an important role in seed germination and early seedling growth in Arabidopsis. Plant Physiol **161:** 165–178

Yoine M, Ohto MA, Onai K, Mita S, Nakamura K (2006) The lba1 mutation of UPF1 RNA helicase involved in nonsense-mediated mRNA decay causes pleiotropic phenotypic changes and altered sugar signalling in Arabidopsis. Plant J **47:** 49–62

Zahler AM, Lane WS, Stolk JA, Roth MB (1992) SR proteins: a conserved family of pre-mRNA splicing factors. Genes Dev **6:** 837–847

Zanetti ME, Chang IF, Gong F, Galbraith DW, Bailey-Serres J (2005) Immunopurification of polyribosomal complexes of Arabidopsis for global analysis of gene expression. Plant Physiol **138:** 624–635

Zhang XN, Mount SM (2009) Two alternatively spliced isoforms of the Arabidopsis SR45 protein have distinct roles during normal plant development. Plant Physiol **150:** 1450–1458

Zhang Y, Gu L, Hou Y, Wang L, Deng X, Hang R, Chen D, Zhang X, Zhang Y, Liu C, Cao X (2015) Integrative genome-wide analysis reveals HLP1, a novel RNA-binding protein, regulates plant flowering by targeting alternative polyadenylation. Cell Res **25:** 864–876

Zhao L, Kunst L (2016) SUPERKILLER complex components are required for the RNA exosome-mediated control of cuticular wax biosynthesis in Arabidopsis inflorescence stems. Plant Physiol **171:** 960–973